Complementary Two-Particle Correlation Observables for Relativistic Nuclear Collisions

Mary Cody,[1,] Sean Gavin,[2,y] Brendan Koch,[1,3,z] Mark Kocherovsky,[1,x] Zoulfekar Mazloum,[2,{] and George Moschelli[1,]

[1]Department of Natural Sciences, Lawrence Technological University, 21000 West Ten Mile Road, Southeld, MI 48075

[2]Department of Physics and Astronomy, Wayne State University, Detroit, MI, 48202

[3]Duke University Medical Center, Durham, Durham, NC, USA

(Dated: January 31, 2022)

Two-particle correlations are a widely used tool for studying relativistic nuclear collisions. Multiplicity uctuations comparing charge and particle species have been studied as a possible signal for Quark-Gluon Plasma (QGP) and the QCD critical point. These uctuation studies all make use of particle variances which can be shown to originate with a two-particle correlation function. Momentum correlations and covariances of momentum uctuations, which arise from the same correlation function, have also been used to extract properties of the nuclear collision medium such as the shear viscosity to entropy density ratio, the shear relaxation time, and temperature uctuations. Searches for critical uctuations are also done with these correlation observables. We derive a mathematical relationship between several number and momentum density correlation observables and outline the dierent physics mechanisms often ascribed to each. This set of observables also contains a new multiplicity-momentum correlation. Our mathematical relation can be used as a validation tool for measurements, as a method for interpreting the relative contributions of dierent physics mechanisms on correlation observables, and as a test for theoretical and phenomenological models to simultaneously explain all observables. We compare an independent source model to simulated events from PYTHIA for all observables in the set.

I. INTRODUCTION

We present a set of two-particle number density and transverse momentum correlation observables that each separately test dierent aspects of relativistic heavy-ion collisions, but are mathematically connected through a parent correlation function. Several observables in the set have previously been measured individually, but are rarely measured simultaneously under the same collision system, energy, and acceptance conditions. One observable, multiplicity-momentum correlations, is new. The mathematical connection between the observables allows any one to be described as a combination of the others, signaling the relative contributions of the physical mechanisms of each. This connection also poses a challenge for models to address all observables simultaneously. In this paper, we outline the construction and interpretation of the individual observables, demonstrate their mathematical connection, and compare a simple independent source model to simulated data.

Two-particle correlation observables are widely used to study aspects of relativistic heavy-ion collisions. Multiplicity uctuations have been linked to centrality or volume uctuations and studied as a possible signal for Quark-Gluon Plasma (QGP) [1{16]. Transverse momentum correlations, in the form of a covariance of two dier-ent particle's traverse momentum uctuation away from the global average, have also been examined as a signa-ture of critical uctuations and linked to event-by-event temperature uctuations [17{30]. In past work, we argue that these correlations result from initial state correlations modied by radial ow [31]. We also argue that these correlations can signal the level of thermalization reached by the collision medium [32{34]. In this work, we distinguish correlation of transverse momentum uctuations from other two-particle transverse momentum correlations that were rst dened in Ref. [35] (see Sec. VI) and used there to estimate the shear viscosity to en-tropy density ratio and shear relaxation time [36{44].

Two-particle correlations are dened by a correlation momentum density $r(p_1; p_2)$ for two particles with three-momenta p_1 and p_2. This correlation function is discussed in detail in Sec. II. A major component of this work is the denition of a new two-particle correlation that emerges from $r(p_1; p_2)$ and measures the covariance of event-by-event total transverse momentum and multiplicity. Analytically, we dene these multiplicity-momentum correlations as

$$D = \frac{\int\int r(p_1; p_2)\ (p_{t;1} \quad \langle p_t \rangle)\ d^3p_1 d^3p_2}{\langle N \rangle^2}; \qquad (1)$$

where $p_t \quad \langle p_t \rangle$ is the uctuation of a particle's transverse momentum away from the global event ensemble average, and $\langle N \rangle$ is the event averaged multiplicity. The rst mention of (1) can be found in Ref. [45]. The experimentally measurable from of (1) is discussed in Sec. IV.

mcody@ltu.edu
[y] sean.gavin@wayne.edu
[z] brendan.koch@duke.edu
[x] mkocherov@ltu.edu
[{] zoulfekar.mazloum@wayne.edu
gmoschell@ltu.edu

In Sec. IV we discuss how D will vanish if the only source of multiplicity-momentum correlations is multiplicity fluctuations. Additionally we show that in the Grand Canonical Ensemble, D is also zero in equilibrium. Non-zero values of D could be a sign of incomplete thermalization, and represent correlations born from the particle production mechanism that survive to freeze-out. Interestingly, in Sec. IX, we find that D is not zero in PYTHIA/Angantyr simulations of proton-proton (pp) and nucleus-nucleus (AA) collisions. Also, we find D is comparable in magnitude to correlations of transverse momentum fluctuations, $\langle \delta p_{t1} \delta p_{t2} \rangle$, which have been well measured at both RHIC and LHC. Until this work, we have previously assumed D is zero and this is also assumed in Ref. [37] where ALICE measures two-particle transverse momentum correlations differentially in relative pseudorapidity and relative azimuthal angle.

Correlations of transverse momentum fluctuations,

$$\langle \delta p \, \delta p \rangle = \frac{\int\int \rho_r(p_1, p_2)\, \delta p_{t1} \delta p_{t2}\, d^3p_1 d^3p_2}{\langle N(N-1) \rangle}, \quad (2)$$

probe the same correlations $\rho_r(p_1, p_2)$ and inspired (1). Here $\delta p_t = p_t - \langle p_t \rangle$. This observable was first measured by STAR in Ref. [20], and we relate the analytic form (2) to the experimentally measurable form (12) in Sec. III.

The similarities between the definitions (1) and (2) are not superficial; they are part of a set of observables mathematically connected by the correlation function $\rho_r(p_1, p_2)$ which is observable in the form

$$R = \frac{\int\int \rho_r(p_1, p_2) d^3p_1 d^3p_2}{\langle N \rangle^2}. \quad (3)$$

Multiplicity fluctuation observables like (3) have been widely studied as a measure of volume or centrality fluctuations and as a potential signature for the onset of QGP and QCD critical point fluctuations. We outline these aspects and the experimental measurement of (3) in Sec. V. The dependence of R on volume fluctuations is also informed by its representation in an independent source model which is discussed in Sec. VIII. Volume fluctuations are determined by the fluctuation of sources of particles from event to event.

Transverse momentum correlations,

$$C = \frac{\int\int \rho_r(p_1, p_2)\, p_{t,1} p_{t,2}\, d^3p_1 d^3p_2}{\langle N \rangle^2}, \quad (4)$$

functionally represent a transverse momentum weighted version of (3) and are therefore generated from the same initial state correlations and volume fluctuations that produce (3). However, due to the momentum dependence, (4) is also sensitive to system expansion and equilibrium dynamics. This is discussed in Sec. VI along with discussion of the experimental measurements.

The main result of this work is that multiplicity-momentum correlations, (1), correlations of transverse momentum fluctuations, (2), multiplicity fluctuations, (3), and transverse momentum correlations, (4), are mathematically related by the equation

$$(1 + R)\langle p_t p_t \rangle - C + 2\langle p_t \rangle D + \langle p_t \rangle^2 R = 0. \quad (5)$$

We derive this result in Sec. VII. When each observable is measured individually, (5) provides a previously unknown validation. Additionally, theoretical and phenomenological models that demonstrate good agreement with one observable can now use that comparison as a benchmark for simultaneously addressing the other observables. Importantly, each observable potentially represents a different physics effect, and with (5), one observable can be decomposed into the contributions from each different effect.

In Sec. VIII we calculate Eqs. (1)-(4) in a general independent source model (ISM) then choose wounded nucleon sources as a test case. A deviation of experimental measurement from the ISM may signal novel physics such as incomplete thermalization or the existence of critical fluctuations. In Sec. IX, we compare the ISM to simulated data generated with PYTHIA 8.2 [46] for several collision energies in pp collisions, as well as in AA collisions using the Angantyr model [47]. The Angantyr model for heavy-ion collisions uses a superposition of nucleon-nucleon sub-collision model, similar to the wounded nucleon model, and allows for fluctuating positions of nucleons in the target and projectile nuclei. Additionally, multi-patron interactions and fluctuations exist in individual nucleon-nucleon sub-collisions. PYTHIA and Angantyr do not include any mechanism for collective expansion in pp or AA collisions, therefore our calculations from simulated events provide a direct comparison to ISM results. Furthermore, the lack of collective effects makes the PYTHIA/Angantyr results an important baseline for experimental measurement. Using PYTHIA/Angantyr, we demonstrate the relationship (5), and calculate the first estimate of D, which we find to be non-zero and positive.

II. CORRELATIONS AND FLUCTUATIONS

The construction of two-particle correlation observables begins by defining the two-particle momentum density

$$\rho_2(p_1, p_2) = \rho_1(p_1)\rho_1(p_2) + \rho_r(p_1, p_2). \quad (6)$$

Here $p_{1,2}$ is the three-momentum of particle 1 or 2 in the pair. Single particle and pair momentum densities, $\rho_1(p)$ and $\rho_2(p_1, p_2)$, are the momentum densities of particles for an ensemble of events such that

$$\rho_1(p) = \frac{d\langle N \rangle}{d^3p}, \quad (7)$$

$$\rho_2(p_1, p_2) = \frac{d\langle N \rangle}{d^3p_1 d^3p_2}, \quad (8)$$

and

$$\langle N \rangle = \int \rho_1(p) d^3p \tag{9}$$

$$\langle N(N-1) \rangle = \int\int \rho_2(p_1, p_2) d^3p_1 d^3p_2. \tag{10}$$

The angled brackets represent an average over the events in the ensemble. For any quantity X, the event average is defined as $\langle X \rangle = N_{events}^{-1} \sum_{k=1}^{N_{events}} X_k$. Then, $\langle N \rangle$ is the average number of particles per event, and $\langle N(N-1) \rangle$ is the average number of particle pairs neglecting autocorrelations.

Equation (6) indicates that particle pairs are generated in two ways. First, if pairs are formed from independent particles, i.e. no correlations, then the pair distribution is simply the multiplication of two single particle densities ρ_{11}. Second, correlated pairs are represented by

$$r(p_1, p_2) = \rho_2(p_1, p_2) - \rho_1(p_1)\rho_1(p_2). \tag{11}$$

By construction, correlations vanish in the case of uncorrelated particle emission, when only statistical fluctuations are present.

At this point, we make no assumption about the physical mechanisms that produce the correlations characterized by (11), though many possibilities have been identified. Correlations of particle emission (momentum) angle with respect to an event plane is commonly called "flow" and is characterized by the coefficients v_n of a Fourier fit to the particle azimuthal distribution: $\sum_{n=2} v_n \cos(n[\phi - \Psi_n])$ [48–50]. Since the event plane angle Ψ_n is calculated for each order and is identified with a geometrical shape – $n = 2$ is elliptical, $n = 3$ is triangular, etc. – flow correlations are often called geometrical correlations. Much effort has gone into identifying so-called "non-flow" correlations that include HBT-like femtoscopic correlations [51, 52], resonance decays and final state interactions [53], momentum conservation [54, 55], and jets. In other works, [31, 56, 57], we have proposed that particles created in close spatial proximity develop a momentum correlation due to transverse expansion. We have argued that this mechanism accounts for much of the signal of two-particle correlations. Since this effect is only indirectly tied to an event reaction plane, many would label this effect as a non-flow effect.

Instead of trying to diagnose the relative contributions from different correlation mechanisms in one observable, we propose a collection of observables that originate with (6), are sensitive to different physics, and are all mathematically connected by (5).

It is common in modern studies [29, 36, 37] for experiments to measure correlation and fluctuation quantities differentially in relative azimuthal angle $\Delta\phi = \phi_1 - \phi_2$ and relative pseudorapidity $\Delta\eta = \eta_1 - \eta_2$. It is also common for experiments to measure pairs that are separated by a gap in pseudorapidity larger than $|\Delta\eta| > 1$.

Measuring observables as a function of $\Delta\eta$ allows for the diagnosis of contributions from anisotropic flow. Projections of differential measurements of observables like (2), (3), and (4) onto the $\Delta\eta$ axis all show a similar pattern of two peaks, one at $\Delta\eta = 0$ and one at $\Delta\eta = \pi$ that is characteristic of both momentum conservation and anisotropic flow. These observables also show a broader peak at $\Delta\eta = \pi$ in comparison to the narrower peak at $\Delta\eta = 0$. This observation is often attributed to the existence of triangular flow.

Pseudorapidity gaps between pairs are used to eliminate "short-range", $|\Delta\eta| < 1$, correlations such as resonance decays and jets. Separately, in differential measurements, HBT and track pileup effects are often removed by eliminating the $\Delta\eta = 0$ bin. Projections onto the $\Delta\phi$ axis of the differential measurements of (2), (3), and (4) all show a "long-range", $|\Delta\eta| > 1 - 2$, correlation in central collisions. This long-range "near-side" ($\Delta\phi = 0$) correlation appears to extend beyond detector rapidity acceptances. Thus, the near-side peak is often described as a peak sitting on a long and flat pedestal, commonly called "the ridge". Experimental measurements often fit the ridge with a Fourier series like $\sum_{n=2} a_n \cos(n\Delta\phi)$ that is fit in $\Delta\phi$ and then relate the a_n coefficients to the v_n anisotropic flow harmonics [28, 29, 37, 41, 58]. The peak sitting on the pedestal represents correlations in excess of the ridge (in excess of flow correlations) and still extends to long-range in $\Delta\eta$ (and possibly beyond the experimental acceptance) in central collisions. The broadness in $\Delta\eta$ of this excess decreases as collisions become more peripheral. Peripheral peaks have widths between $0.5 - 1$, which are consistent with jet and resonance decay correlations. The increasing width of the near side peak from peripheral to central collisions indicates that a correlation mechanism that is not attributed to flow harmonics is at work. See, for example, Ref. [42].

If the observables (2), (3), and (4) are not measured differentially in $(\Delta\eta, \Delta\phi)$, then all flow effects are eliminated. To understand this, imagine the quantity $R(\Delta\phi)$ has been measured and is well described by a Fourier series with terms $a_n \cos(n\Delta\phi)$. To find the integrated quantity, one calculates $R = \int_0^{2\pi} R(\Delta\phi) d\Delta\phi$. When calculating the equivalent integral of the Fourier series, the integral of all terms $\cos(n\Delta\phi)$ over a symmetric interval vanish term by term, indicating $R = 0$ if correlations are only described by flow. Therefore, if the integrated quantity R is not zero, it is not fully explained by Fourier flow coefficients. Although these remaining correlations might be characterized as non-flow, they are still interesting and potentially provide useful information about the collisions dynamics or initial state. In particular, we highlight the near-side correlations in excess of flow that are long-range in nature. Additionally, if jet effects dominate the integrated observables, the different observables (1)-(4) analyzed together may be able to distinguish classes of events based on jet properties. Alternatively, the centrality and system energy dependence of these correlations can indicate the level of thermalization of events, which we leave to future work.

Correlations (11) also indicate the event-by-event fluc-

tuations in produced particles. Notice that integrating (11) over all momenta for both particles results in $\langle N(N-1)\rangle - \langle N\rangle^2 = Var(N) - \langle N\rangle$. Here the variance of particles, $Var(N) = \langle N^2\rangle - \langle N\rangle^2$, characterizes the fluctuation in produced particles. If each event is independent of all other events, then this variance should follow Poisson statistics – where the variance is equal to the mean – resulting in a vanishing integral of (11).

Non-Poissionian fluctuations indicate that a physical mechanism – in initial state production, the dynamical expansion, or final state interactions – generates fluctuations in a correlated way in all of the events of the ensemble; in this case $r(p_1; p_2) = 0$. Consequentially, since these fluctuations are tied to physical processes, they are not completely random and can be identified with correlation observables. Non-Poissionian behavior is seen in experiments as well as simulations, and will be discussed in the next sections.

III. CORRELATIONS OF TRANSVERSE MOMENTUM FLUCTUATIONS

Transverse momentum correlations in excess of multiplicity fluctuations, defined by (2), have been widely studied as a possible signal for the existence of QGP [17–30]. QCD critical point searches look for non-monotonic behaviors since fluctuations are expected to diverge if the system passes through a phase transition [6, 59]. Similarly, the event-by-event variation in p_t can be used as a measure of event temperature fluctuations [20, 60].

We focus on momentum correlations defined by (2), which are experimentally measurable with

$$\langle p_{t1}p_{t2}\rangle = \frac{\left\langle \sum_{i=1}^{N_k}\sum_{j=1;j\neq i}^{N_k} p_{t;i}p_{t;j} \right\rangle}{\langle N(N-1)\rangle}; \tag{12}$$

where

$$p_{t;i} = p_{t;i} - \langle p_t\rangle \tag{13}$$

is the fluctuation of the transverse momentum of particle i in event k from the global average transverse momentum per particle, $\langle p_t\rangle$, for a given centrality class. Since (13) is a fluctuation, (12) is a covariance of fluctuations. In this work, we distinguish correlations of transverse momentum fluctuations (12) from transverse momentum correlations in Sec. VI to avoid confusion. We will discuss the relationship between these two types of momentum correlations in Sec. VII.

$\langle p_{t1}p_{t2}\rangle$ measures the covariance of transverse momentum fluctuations away from the global average. When two particles both have larger or smaller p_t than the average, that pair contributes positively to $\langle p_{t1}p_{t2}\rangle$. When one particle of a pair has positive p_t and the other has negative p_t, then that pair contributes negatively to $\langle p_{t1}p_{t2}\rangle$. In the case of purely independent particle emission, $\langle p_{t1}p_{t2}\rangle = 0$.

The definition (12) differs slightly from definitions found in experimental measurements. Experiments measure

$$\langle p_{t1}p_{t2}\rangle = \frac{1}{N_{event}}\sum_{k=1}^{N_{event}}\frac{C_k}{N_k(N_k-1)} \tag{14}$$

with

$$C_k = \sum_{i=1}^{N_k}\sum_{j=1;j\neq i}^{N_k}(p_{t;i} - M_{p_t})(p_{t;i} - M_{p_t}) \tag{15}$$

and

$$M_{p_t} = \frac{1}{N_{event}}\sum_{k=1}^{N_{event}}\langle p_t\rangle_k \tag{16}$$

where $\langle p_t\rangle_k$ is the average transverse momentum in event k,

$$\langle p_t\rangle_k = \frac{1}{N_k}\sum_{i=1}^{N_k} p_{t;i}. \tag{17}$$

There are two differences. First, the average transverse momentum (16) is calculated event-by-event such that the average transverse momentum per particle of each event is found first then averaged over all events in the same centrality class. In (12) we define the average transverse momentum per particle as

$$\langle p_t\rangle = \langle P_T\rangle / \langle N\rangle. \tag{18}$$

where

$$\langle P_T\rangle = \left\langle \sum_{i=1}^{N_k} p_{t;i} \right\rangle = \int n_1(p)\, p_t\, d^3p; \tag{19}$$

which is more representative of our theoretical description of the momentum density (7). The second difference between (12) and (14) is in the normalization. The denominator of (12) is calculated independently, where the ratio $C_k/N_k(N_k-1)$ is calculated event-by-event in (14). We make this choice in (12) to maintain as much consistency as possible between (2) and (1), (3), and (4). In Fig. 1 we plot both (12) and (14) calculated with the same PYTHIA events. Excellent agreement is observed.

Experiments report positive values of $\langle p_{t1}p_{t2}\rangle$ in pp and AA collisions at various energies. $\langle p_{t1}p_{t2}\rangle$ decreases with centrality, but not quite following $1/\langle N\rangle$ [20, 26, 30]. If $\langle p_{t1}p_{t2}\rangle$ falls with $1/\langle N\rangle$, then the quantity $(dN/d)\langle p_{t1}p_{t2}\rangle$ should be approximately flat. However, experimental measurements of $(dN/d)\langle p_{t1}p_{t2}\rangle$ rise from peripheral to mid-peripheral collisions and plateau toward more central collisions. This rise could signal the onset of critical fluctuations [20, 26] or the effects of incomplete thermalization [34]. It is common for experimental measurements to report $\langle p_{t1}p_{t2}\rangle$ as a relative dynamical correlation

$$\sqrt{\langle p_{t1}p_{t2}\rangle}/\langle p_t\rangle; \tag{20}$$

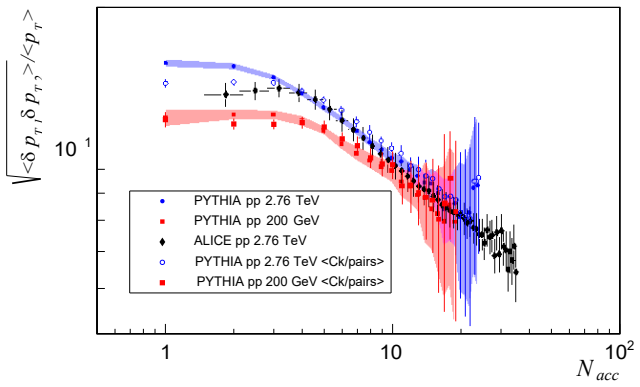

FIG. 1. Comparison of Eq. (20) calculations from PYTHIA pp events (circles and squares) with measurement from ALICE (solid diamonds) [26, 27]. Solid circles and squares represent (12), while open circles and squares represent (14).

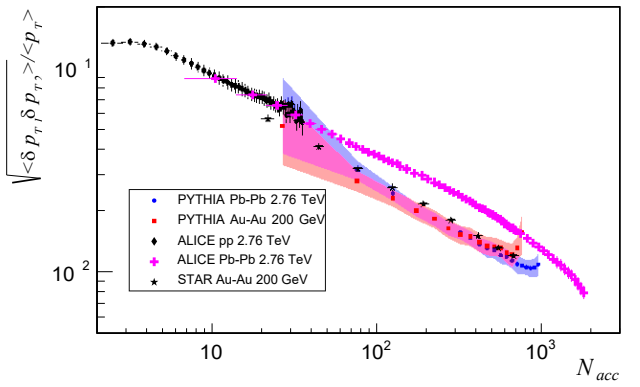

FIG. 2. Comparison of Eq. (12) calculations from PYTHIA AA events with measurement from ALICE pp and Pb-Pb collisions [26, 27], and STAR Au-Au collisions [30]. Centrality is determined by multiplicity.

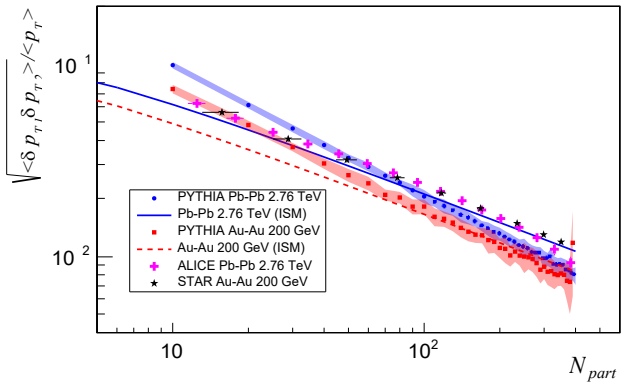

FIG. 3. Comparison of Eq. (12) calculations from PYTHIA AA events with measurement from ALICE pp and Pb-Pb collisions [26, 27], and STAR Au-Au collisions [30]. Centrality is determined by the number of participating nucleons. Solid lines represent the independent source model for wounded nucleons, Eq. (57).

which is dimensionless. It also rescales the growth of (12) to be dependent on the cumulative eect of correlations rather than the size of $\langle p_t \rangle$. This scaling nearly removes the collision energy dependence of the measurements [20, 26, 30]. Using PYTHIA/Angantyr simulated events, we calculate (20) using (12) and (18), and compare to experimental data in Figs. 1, 2, and 3. Details are discussed in Sec. IX.

As with R and C, experiments measure $\langle p_{t1} p_{t2} \rangle$ differentially in relative rapidity and relative azimuthal angle (;). The ALICE collaboration measures the quantity $P_2(;) = \langle p_{t1} p_{t2} \rangle(;)/\langle p_t \rangle^2$ which shows the characteristic ridge-like shape for charge inde-pendent correlations [29]. The near-side ridge at = 0 is not completely explainable with Fourier decomposi-tion, and excess correlations appear to be long-range in . Short range eects like resonance decays and jets can produce positive correlations in $\langle p_{t1} p_{t2} \rangle$, but they cannot fully explain the excess long range correlations seen in $P_2(;)$.

Several explanations for these correlations have been proposed. They include the quark coalescence models [61], string percolation models where clustered strings produce colored sources [62], uctuations in event size and entropy [63], and a boosted source model where correlations originating in initial state hot-spots are enhanced by radial ow [31]. We propose that any explanation of these correlations, should simultaneously address other two-particle correlations that originate from (11) such as (1), (3), and (4).

IV. MULTIPLICITY-MOMENTUM CORRELATIONS

A new observable D, dened by (1), tests the correlation of transverse momentum with particle production event-by-event. In Sec. IX we show that in PYTHIA/Angantyr simulations D is generally positive and comparable in magnitude to $\langle p_{t1} p_{t2} \rangle$.

In (1), p_t is dened by (13), and $\langle p_t \rangle$ is the average transverse momentum per particle for a given centrality class of events (18). Experimentally, (1) can be measured with the nal state particle pair sum

$$D = \frac{\left\langle \sum_{i=1}^{N_k} \sum_{j=1;j=i}^{N_k} p_{t;i} \right\rangle}{\langle N \rangle^2} = \frac{\left\langle (N_k - 1) \sum_{i=1}^{N_k} p_{t;i} \right\rangle}{\langle N \rangle^2}: \quad (21)$$

To understand this observable, we expand $p_{t;i}$ in the middle term of (21) with (13) and substitute

$$\left\langle \sum_{i=1}^{N_k} \sum_{j=1;j=i}^{N_k} p_{t;i} \right\rangle = \langle P_T N \rangle - \langle P_T \rangle \quad (22)$$

and

$$\left\langle \sum_{i=1}^{N_k} \sum_{j=1;j=i}^{N_k} \right\rangle = \langle p_t \rangle \langle N(N-1) \rangle: \quad (23)$$

Adding and subtracting $\langle P_T\rangle\langle N\rangle$ and making use of the fact that (18) can be written as $\langle P_T\rangle = \langle p_t\rangle\langle N\rangle$, we find

$$D = \frac{\mathrm{Cov}(P_T, N) \quad \langle p_t\rangle \mathrm{Var}(N)}{\langle N\rangle^2}; \tag{24}$$

where $\mathrm{Cov}(P_T, N) = \langle P_T N\rangle \quad \langle P_T\rangle\langle N\rangle$ is the covariance of total transverse momentum P_T and multiplicity N per event. The event multiplicity variance is $\mathrm{Var}(N) = \langle N^2\rangle \quad \langle N\rangle^2$.

Since every particle carries some transverse momentum, adding any particle to an event will increase the total transverse momentum in that event. Therefore, a natural correlation between total p_t and multiplicity exists that is dominated purely by multiplicity fluctuations. Notice this contribution is subtracted by the rightmost term of (24). This indicates that D should be zero if multiplicity fluctuations are the only source of multiplicity-momentum correlations.

In the Grand Canonical Ensemble, we can follow Ref. [45] to show that D should vanish in equilibrium. In equilibrium, the Grand Partition Function with chemical potential , volume V, and temperature T, is $Z(\ ; V; T) = \sum_i \exp(N_i \quad E_i)$. Here the Gibbs factor - with number of particles N_i and energy E_i of state i - is summed over all states. We define $\quad = \ /T$ and $\ = 1/T$ and take the Boltzmann constant to be in natural units $k_B = 1$. The average number of particles and average energy are found in the usual way

$$\langle N\rangle = \sum_i N_i \frac{e^{N_i E_i}}{Z} = \frac{1}{Z}\frac{\partial Z}{\partial}; \tag{25}$$

$$\langle E\rangle = \sum_i E_i \frac{e^{N_i E_i}}{Z} = \frac{1}{Z}\frac{\partial Z}{\partial}. \tag{26}$$

Second derivatives in yield

$$\frac{\partial\langle N\rangle}{\partial_i} = \sum_i \frac{N_i e^{N_i E_i}}{Z} \quad \frac{e^{N_i E_i}}{Z^2}\frac{\partial Z}{\partial} = \langle N^2\rangle \quad \langle N\rangle^2; \tag{27}$$

$$\frac{\partial\langle E\rangle}{\partial_i} = \sum_i \frac{N_i e^{N_i E_i}}{Z} \quad \frac{e^{N_i E_i}}{Z^2}\frac{\partial Z}{\partial} = \langle N E\rangle \quad \langle N\rangle\langle E\rangle = \frac{\partial\langle E\rangle}{\partial\langle N\rangle}\frac{\partial\langle N\rangle}{\partial}. \tag{28}$$

Defining $D_E = (\mathrm{Cov}(E; N) \quad "\mathrm{Var}(N))/\langle N\rangle^2$ where $" = \langle E\rangle/\langle N\rangle$, we find that D_E vanishes when the energy per particle satisfies $" = \partial\langle E\rangle/\partial\langle N\rangle$.

To relate energy and transverse momentum fluctuations, we take the transverse mass to be $m_t = \sqrt{m^2 + p_t^2}$ p_t for particles with large momentum, p_t m. Near mid-rapidity $y \ 0$, the energy $E_i = m_{t;i}\cosh y_i \ m_{t;i}$ $p_{t;i}$ averaged over states is then approximately the average total transverse momentum $\langle E\rangle \ \langle P_T\rangle$. Following that, we substitute $\partial\langle E\rangle/\partial\langle N\rangle = \partial\langle P_T\rangle/\partial\langle N\rangle$ in the last term of (28). In the case where $\langle p_t\rangle$ is constant over a wide range of multiplicities, the definition $\langle P_T\rangle = \langle p_t\rangle\langle N\rangle$, Eq (18), yields $\partial\langle P_T\rangle/\partial\langle N\rangle \ \langle p_t\rangle$. Using this result in (28) with (27), we find

$$\langle N P_T\rangle \quad \langle N\rangle\langle P_T\rangle = \langle p_t\rangle(\langle N^2\rangle \quad \langle N\rangle^2): \tag{29}$$

Finally, substituting (29) in (24), we find that $D = 0$.

Several factors may generate a non-zero D. Hadronization may violate the assumption that p_t m for all particles. For example, in $\sqrt{s} = 200$ GeV collision systems, the average transverse momentum is approximately $\langle p_t\rangle \ 0{:}5$ GeV , which is arguably large compared to the pion mass, but not the kaon or proton masses. Heavier particles may skew the momentum-multiplicity covariance $\mathrm{Cov}(P_T\ ; N)$. Particle rapidities greater than $|y| > 0{:}5$ have increasingly larger deviations from our $y = 0$ assumption. If higher momentum particles, say with $p_t > 2$ GeV , come at the cost of producing fewer particles near the average momentum, then the covariance $\mathrm{Cov}(P_T\ ; N)$ would become negative. If high momentum particles come in conjunction

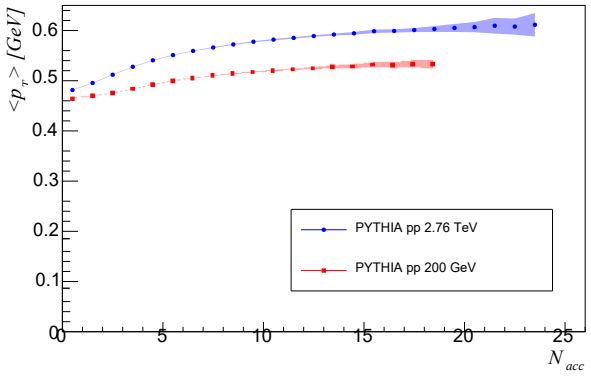

FIG. 4. Average transverse momentum per particle as a function of reference multiplicity for pp collisions at select energies. Error bars on the PYTHIA results represent statistical uncertainty.

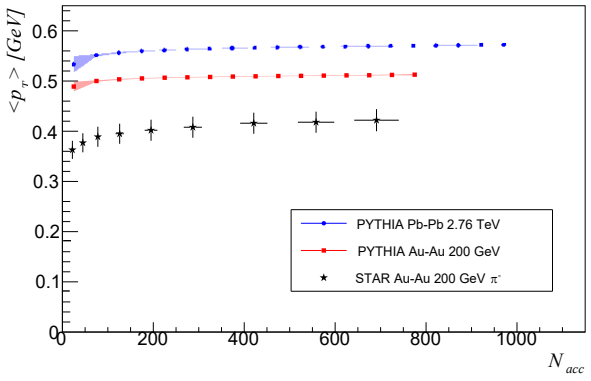

FIG. 5. Average transverse momentum per particle as a function of reference multiplicity for select AA collision systems. Error bars on the PYTHIA results represent statistical uncertainty. STAR data is from [64].

with excess particles near the average, then the covariance $Cov(P_T; N)$ will be positive. Lastly, the assumption $@hP_Ti=@hNi\ hp_ti$ does not hold if transverse momentum per particle increases with increasing event multiplicity.

Examining hp_ti vs. multiplicity, Figs. 4 and 5, we notice that the average transverse momentum per particle increases with event multiplicity. This is seen across collision systems and energies. See, for example, Ref. [65]. This is a positive transverse momentum and multiplicity covariance, if only a slight one. Possible sources of this covariance include jet particle production or an increased radial flow velocity in central collisions in comparison to peripheral collisions. This increase in hp_ti has been seen in PYTHIA and is considered a consequence of the multiple interaction model [66] and color reconnection [67]. In all of these cases, non-zero D indicates a correlation related to particle production and dynamics that is distinct from R, C, and $hp_{t1}p_{t2}i$. We will show in Sec. VII, how correlations D contribute to the other observables C and $hp_{t1}p_{t2}i$.

V. MULTIPLICITY FLUCTUATIONS

Multiplicity fluctuations have been widely studied with the goal of signaling the onset of QGP. Net charge fluctuations are used to distinguish QGP from hadron gas [1–4]. Such studies rely on the idea of "volume fluctuations" to connect event selections based on multiplicity to a geometric picture of the collision region [5]. Other net charge fluctuation studies look for large divergences that could signal a QGP phase transition [6–8]. Inclusive multiplicity fluctuations have been linked to the isothermal compressibility of the system [9–11] assuming the mid-rapidity region can be described by the Grand Canonical Ensemble. (A study intended to be used as a baseline of statistical fluctuations emerging from a hadron-resonance gas in the Canonical, Micro Canonical, and Grand Canonical Ensembles can be found here [12].) Net baryon fluctuations are used to identify small regions of chiral condensates to classify events that signal QGP formation [13, 14]. All of these references use observables constructed of moments of inclusive or identified particle multiplicities [15, 16].

In this section we outline aspects of the multiplicity fluctuation observable (3) that is measurable as

$$R = \frac{hN(N-1)i - hNi^2}{hNi^2} = \frac{Var(N) - hNi}{hNi^2}; \qquad (30)$$

[16]. We discuss how R sets an overall scale for any two-particle correlation that can be derived from the correlation function (11). Due to this connection, we examine how the construction of R yields a characteristic $1=hNi$ behavior that influences the interpretation of every two-particle correlation observable included in this paper.

In Ref. [16], Pruneau et al. show that, for inclusive distributions, the observable R is robust against detection efficiency effects and acceptance limitations. To show this, we start by constructing (30) from the single particle distribution, $_1$, and pair distribution, $_2$, using (9) and (10) and follow arguments from both Refs. [16] and [31]. If (9) and (10) are given arbitrary normalizations a and b such that we have $_2 \to a_2$ and $_{11} \to b_{11}$, then (30) becomes

$$R_{acc} = \frac{a}{b}R + \frac{a-b}{b}. \qquad (31)$$

If $a = b$, then R will receive a scale and offset that could be detector and collision system and energy dependent. However, if a and b are equal, such as the case for detector tracking efficiency, then $R = R_{acc}$. This motivates the choice to normalize R by hNi^2.

Consequentially, examining the rightmost definition of R in (30), notice that if both terms in the numerator have a scale of hNi, then R will follow a $1=hNi$ behavior. This is the case if the multiplicity distribution follows a binomial or negative binomial distribution. For independent particle production, the multiplicity distribution follows Poisson statistics and the variance equals the mean and $R = 0$. In Sec. VIII, we show that in an independent source model, all of the observables constructed similar to (3) trend like hKi^{-1} where K is the number of sources in an event. This $1=hNi$ or $1=hKi$ behavior is a defining characteristic of these correlations and therefore we look for deviations from this trend.

In the search for critical fluctuations, the PHENIX collaboration measured the scaled variance of the charged multiplicity

$$! = \frac{hN^2i - hNi^2}{hNi} = \frac{^2}{} \qquad (32)$$

where $hNi =$ is the average charged particle multiplicity and $^2 = hN^2i - hNi^2$ is the variance [10]. The multiplicity distribution of heavy ion collisions follow a Negative Binomial Distribution (NBD) with mean and scaled variance $! = 1 + =k_{NBD}$, where k_{NBD} is a parameter. The NBD parameter is related to (30) by

$$R = \frac{^2 - }{^2} = ! - \frac{1}{k} = \frac{1}{DNB}. \qquad (33)$$

Subsets of a NBD, randomly sampled with constant probability, will have the same k_{NBD}. Let and ! be the mean multiplicity and scaled variance from an unlimited acceptance. Also let $_{acc}$ and $!_{acc}$ be the mean and scaled variance from a fractional acceptance. By Definition, the scaled variance for fractional acceptance is then $!_{acc} = 1 + _{acc}=k_{NBD}$. Using $R = k^{-1}_{NBD}$ and the relation (33) for $_{acc}$ and $!_{acc}$, we find $R = (!_{acc} - 1)=_{acc} = R_{acc}$, since k_{NBD} is identical for the full acceptance and fractional acceptance regions. This result is consistent with (31) for $a = b$, and makes R an ideal measure of the strength of correlations.

Importantly, multiplicity fluctuations R set the scale for all two-particle correlation observables that depend

on $r(p_1; p_2)$, Eq. (11), since correlations are related to (30) by (3). These correlations come from many sources beginning with initial state energy deposition. Thermal \hot spots" emit particles in a fundamentally dierent way from perturbative QCD processes like jets. Particularly, the dierent energy scale constrains the yields of more massive mesons and baryons. However, uctuating temperatures of dierent hot spots or uctuating num-bers of hard scatterings both add a contribution from source uctuations to (3). See Sec. VIII. Final state ef-fects, like resonance decays and hadronization also yield multiparticle correlations.

Dierential studies of (30) led to the discovery of the ridge, which shows that correlations extend to large separations in rapidity [29, 68{71] and the strength of these long range correlations is dictated by (11) [57, 72, 73]. Various explanations attribute the appearance of the ridge to ow or other correlations modied by ow [56, 74], but this kind of bulk correlation of particle mo-menta due to the transverse collision geometry shifts the location of particles in phase space but does not change the yields of particles. As discussed in Sec. II, a geomet-rical correlation alone would yield a value of $R = 0$ when integrated.

When investigating the centrality dependence of multiplicity uctuations (30), biases are introduced if the same particles are used to measure correlations and measure centrality. This will be discussed in detail in Sec. IX, however, it is informative to briey discuss one aspect here. Imagine (30) was calculated from events with exactly the same number of particles. Then, $hN^2i = hNi^2$ and

$$R \; ! \quad \frac{1}{hNi}: \tag{34}$$

This shows a limiting behavior that is a response to multiplicity binning. To avoid this eect, the multiplicity used to measure centrality must be dierent from the multiplicity used to calculate (30). Additionally, to have a positive R, the multiplicity variance must be larger than hNi. To deviate from a $1=hNi$ behavior, the multiplicity variance must also change faster or slower than hNi with increasing centrality.

VI. TRANSVERSE MOMENTUM CORRELATIONS

Two-particle transverse momentum correlations, (4), are measurable as

$$C = \frac{\left\langle \sum_{i=1}^{N_k} \sum_{j=i}^{N_k} p_{t;i} p_{t;j} \right\rangle - hP_T i^2}{hNi^2}; \tag{35}$$

where the rightmost term is (19), the event averaged total transverse momentum per event.

The momentum correlation observable (35) was rst dened in Ref. [35] as part of a method for extract-ing the shear viscosity to entropy density ratio, $=s$, independently from ow harmonic measurements. STAR measured C, for the rst time, dierentially in relative pseudorapidity and relative azimuhtal angle $C(;)$ [36]. This measurement constrained $=s$ to a range of $0:06 < =s < 0:21$ which is in agreement with hydrodynamic ow estimates and the predicted AdS/CFT lower limit of $=s = 1=4$ [75]. The measured range is due mostly to experimental systematic uncertainty which may be reducible by measuring the integrated form of the rapidity width of (35) like $^2 = \int_C C()^2 d$ without using any t functions. ALICE measures a slightly mod-ied form of (35) dened as $G_2 = C=hp_t i^2$ [37{40]. The dierential form of G_2 was recently used in [41] to extract harmonic Fourier coecients in from simulated data and compare them to harmonic ow coecients v_n mea-sured with the cumulant method and a pseudorapidty gap of $jj = 0:7$.

Momentum correlations (35) are sensitive to both number density uctuations as well as transverse momentum uctuations; both are necessary to address the diusion of transverse momentum uctuations due to shear viscosity. Reference [35] predicts that the simultaneous diffusion and dampening of initial state momentum uctuations due to shear viscous forces results in the broadening of correlations C in relative rapidity over the collision lifetime. Since central collisions have longer lifetimes than peripheral ones, a centrality dependent measurement of the relative rapidity width of C should show a monotonic increase. This behavior was rst seen by STAR when they measured (35) dierentially in relative pseudorapidity and relative aziumuthal angle $C(;)$ [36].

STAR found a dierential correlation structure similar to the ridge, $R(;)$, with a near-side peak at $= 0$ that is broad in and an away-side peak at $=$ that is at in . The double peaks in are commonly seen as an indication of hydrodynamic ow because they can be (mostly) characterized by a Fourier cosine series. However, on the near-side, correlations in excess of the Fourier t exist and are peaked at $= = 0$. In pe-ripheral collisions these excess correlations have a narrow prole in that is consistent with resonance decay or jet correlations. As collisions become more central, the rapidity width of excess correlations increases in agree-ment with [35].

Unexpectedly, Ref. [36] found that the rapidity broadening of the near side of $C(;)$ was not Gaussian in nature. Instead, central collisions had two peaks in with a local minimum at $= 0$. In Refs. [42{44] we argue that the non-Gaussian broadening is a signal of causal diusion that depends on both the shear viscosity and the shear relaxation time.

We can see how (35) incorporates number density uctuations by writing it in terms of the correlation function (11) to nd (4). Comparing (4) to (3), notice that all multiplicity uctuations in (35) are the same as those in (30),

except they are weighted by transverse momentum. This is important because every particle carries some momentum, and therefore correlations and diusion of particles necessarily implies correlations and diusion of momentum. In larger multiplicity events, more momentum pairs are possible. Higher multiplicity events also have longer lifetimes which allow for correlations to develop due to dynamic processes like geometric ow, but longer lifetimes also allow more time for equilibration which destroys correlations.

We discuss transverse momentum correlations with number density uctuations removed in Sec. III, but C was designed to probe the transfer of transverse momentum correlations between two points in the QGP { from small rapidity separation to larger separations { and number density uctuations are a part of that process. For example, imagine an event with a uctuating initial state. In a hydrodynamic or kinetic theory picture, hot and cold spots are deposited throughout the collision volume each with a dierent local temperature and energy density. Movement toward equilibrium is driven, in part, by viscous forces transferring energy density or momentum density or particle number density from higher temperature spots to lower ones. Interestingly, shear viscosity transports momentum perpendicular to the direction of ow, therefore shear viscosity spreads transverse momentum uctuations in the longitudinal direction. That momentum can be spread by microscopic parton collisions as well as by transmission of number density.

Momentum correlations emerge form the initial state because pairs of particles are emitted from the same source and are generally subject to local enforcement of conservation laws. Since particles originate at the same spatial location, they experience roughly the same dynamics and can develop new correlations with each other and with the global event plane due to transverse expansion [31, 56, 57, 76]. Additionally, if correlations exist over rapidity ranges of jj > 1 2 units then causal-ity requires that they develop at the early stages of the collisions [77]. If momentum correlations originate because pairs of particles are emitted from the same source, then the number of correlated pairs is roughly proportional to the temperature of the source. The more pairs, the stronger the correlation. In equilibrium, the distinction between dierent sources is destroyed, reducing the strength of the correlation.

VII. COMPLIMENTARY FLUCTUATION AND CORRELATION OBSERVABLES

The observables $\langle p_{t1}p_{t2}\rangle$, (12), D, (21), R, (30), and C, (35), are mathematically related based on their com-mon origin (11) and the denition of a transverse mo-mentum uctuation p_t, (13). We nd the relation (5).

Starting from the denition (12) we expand the argument $p_{t;i}p_{t;i}$, to nd

$$\langle p_{t1}p_{t2}\rangle = \frac{\sum_{i=1}^{N_k}\sum_{j=i}^{N_k} p_{t;i}p_{t;j} - p_{t;i}\langle p_t\rangle - p_{t;j}\langle p_t\rangle + \langle p_t\rangle^2}{\langle N(N-1)\rangle}. \quad (36)$$

Applying the sums over pairs, we nd

$$\begin{aligned}\langle N(N-1)\rangle\langle p_{t1}p_{t2}\rangle = &\\ &= \langle N\rangle^2 C + \langle P_T\rangle^2 && (37a)\\ &\quad 2(\langle P_T N\rangle - \langle P_T\rangle)\langle p_t\rangle && (37b)\\ &+ \langle p_t\rangle^2\langle N(N-1)\rangle. && (37c)\end{aligned}$$

Using (35), the rst term of (36), becomes (37a). The middle two terms in (36) both become $(\langle P_T N\rangle - \langle P_T\rangle)\langle p_t\rangle$ after using (22), resulting in (37b). The last term of (36) yields (37c), similarly to (23). After adding and subtracting $2\langle p_t\rangle\langle P_T\rangle\langle N\rangle + 2\langle p_t\rangle^2\langle N^2\rangle$ to (37), we make use of denitions (24) and (30) to construct

$$\langle p_{t1}p_{t2}\rangle = \frac{C - 2\langle p_t\rangle D - \langle p_t\rangle^2 R}{(1+R)}; \quad (38)$$

where $(1+R) = \langle N(N-1)\rangle/\langle N\rangle^2$.

The denominator of (38) is a result of the dierent normalization of (12) compared to (21), (30), and (35). To facilitate direct comparison to measured data, we choose not to alter the normalization of $\langle p_{t1}p_{t2}\rangle$. However, (38) requires the denition of $\langle p_{t1}p_{t2}\rangle$ to be (12) rather than (14). We show that this change has small eect on measurement in Fig. 1.

Equation (38) is equivalent to (5) and is a primary result of this paper. From (38), we see that correlations of transverse momentum uctuations can be interpreted as transverse momentum correlations with multiplicity uctuations removed ($C - \langle p_t\rangle^2 R$) only if multiplicity-momentum correlations, D, are zero.

Assuming D is small, the dierence $C - \langle p_t\rangle^2 R$ highlights the construction of $\langle p_{t1}p_{t2}\rangle$. Notably, C is at least an order of magnitude larger than $\langle p_{t1}p_{t2}\rangle$, which indi-cates multiplicity uctuations, R, dominate momentum correlations, C. Nonetheless, $\langle p_{t1}p_{t2}\rangle$ measurements are positive and non-zero, which indicates that momen-tum correlations are generated by some physics mecha-nism that is not explainable by multiplicity uctuations. Any theoretical or phenomenological explanation of that mechanism must address both the cause of correlations and why they are not subtracted by D or R.

In Sec. IX, we calculate values of D in simulated PYTHIA events. We nd that it is on the same order of magnitude as $\langle p_{t1}p_{t2}\rangle$, and possibly even larger. Therefore, D should not be assumed negligible when measuring $\langle p_{t1}p_{t2}\rangle$ or C.

The $1/\langle N\rangle$ (or deviation from $1/\langle N\rangle$) behavior of $\langle p_{t1}p_{t2}\rangle$ can also be studied with (38). Notably, R exhibits the most obvious expression of the $1/\langle N\rangle$ trend { see discussion around Eq. (34) { and, by construction,

C and D are expected to have similar behavior. This is more obvious in an independent source model, which we discuss in Sec. VIII. We test this behavior with simulated events in Sec. IX.

The inuence of $\langle p_t \rangle$ also appears in (5) and (38). Since $\langle p_t \rangle$ is seen to rise with multiplicity, it is a potential source of deviation from $1/\langle N \rangle$ scaling for $\langle p_{t1} p_{t2} \rangle$ that is not due to critical phenomena. Since $\langle p_t \rangle$ also increases with increasing collision energy, experiments tested a scaling (20) for $\langle p_{t1} p_{t2} \rangle$ that shows approximate agreement over a wide range of systems and energies [20, 26, 30]. The quality of the agreement relies somewhat on the choice of centrality measure. In (38), we can see how constituent correlation observables contribute to this scaling and how centrality determination aects this agreement. To avoid interpreting the square root in (20), we instead consider $\langle p_{t1} p_{t2} \rangle = \langle p_t \rangle^2$ and write (5) as

$$\frac{(1 + R)\langle p_{t1} p_{t2} \rangle}{\langle p_t \rangle^2} = \frac{C}{\langle p_t \rangle^2} \quad \frac{2D}{\langle p_t \rangle} \quad R: \qquad (39)$$

Using (39) we can see that scaling with collision energy requires consistent handling of multiplicity uctuation R. Fortunately, if R and C are measured with the same methods, centrality biases in C are subtracted by R. This is what makes $\langle p_{t1} p_{t2} \rangle$ robust against dierent central-ity denitions.

Alternatively, we can study two-particle transverse momentum correlations by rewriting (5), or (38), as

$$C = (1 + R)\langle p_t p_t \rangle + 2\langle p_t \rangle D + \langle p_t \rangle^2 R: \qquad (40)$$

Equation (40) distinguishes the dierent physical inuences on momentum correlations. The rightmost term represents the contribution just from multiplicity uctuations (including volume uctuations). This is the largest contribution to C. In this context the quantitative difference between R and its momentum weighted counterpart C can be measured. C is aected by forces like viscosity that impact temperature uctuations which are represented by the presence of $\langle p_{t1} p_{t2} \rangle$. Similarly, the presence of D signals how C is inuenced by the mechanism that correlates total transverse momentum with multiplicity event-by-event.

The ALICE collaboration measures the dierential quantity $G_2(;) = C(;)/\langle p_t \rangle^2$ [37{40]. Using (39) we nd the integrated version

$$G_2 = \frac{C}{\langle p_t \rangle^2} = \frac{(1 + R)\langle p_{t1} p_{t2} \rangle}{\langle p_t \rangle^2} + \frac{2D}{\langle p_t \rangle} + R; \qquad (41)$$

but each of the terms on the right hand side can also be measured dierentially. For example, the quantities $P_2 = \langle p_{t1} p_{t2} \rangle(;)/\langle p_t \rangle$ and $R_2(;)$ are measured in Ref. [29]. With the measurement of $D(;)/\langle p_t \rangle$, $G_2(;)$ can be checked experimentally, using (41).

To summarize, multiplicity uctuations, R, set an underlying scale of correlations, (11), that is determined by particle production mechanisms, volume uctuations, and possibly phase change uctuations. Momentum correlations, C, indicates both how initial state correlations survive to nal state particle p_t, and how transverse momentum can be transferred throughout the collision volume by forces like shear viscosity. D represents correlations of event-by-event total transverse momentum and multiplicity. Equation (24) demonstrates that these correlations are in excess of those from random multiplicity uctuations, so D is therefore tied to particle production. Furthermore, lack of correlations, D, can signal equilibration while enhancement of D could exist around the QGP critical point. Correlations of uctuations of transverse momentum, $\langle p_{t1} p_{t2} \rangle$, have several theoreti-cal explanations like temperature uctuations or boosted hot spots. Importantly, the results (5), or (38), or (39), or (40), or (41) suggest that a theoretical or phenomenological explanation of one of the observables R, C, D, or $\langle p_{t1} p_{t2} \rangle$ can be tested by separately addressing each of the others. Similarly, with simultaneous experimen-tal measurement of all four observables (12), (21) (30), and (35), Eq. (5) acts both as a validation tool for each measurement and as a way to explicitly distinguish multiplicity uctuations from other correlations mechanisms when looking for critical phenomenon.

VIII. INDEPENDENT SOURCE MODEL

The independent source model assumes that nuclear collision events are comprised of a superposition of independent sources of particles and ignores any interactions between particles emitted from dierent sources. Each event has a uctuating number of sources and each source has a uctuating multiplicity and momentum distribution of particles. In this section we detail how the observables discussed in sections III, IV, V, and VI depend on both of these types of uctuation. A similar discussion for only R and $\langle p_{t1} p_{t2} \rangle$ appears in Ref. [31]. Our independent source model assumes that a sin-gle collision event is the sum of K independent particle sources. Each source is represented by a momentum distribution $\hat{}_1(p)$ normalized such that $\int \hat{}_1(p) d^3p =$ is the mean multiplicity per source. To understand the average particle distribution of sources, imagine a large number of sources running from $k = 1; :::; N_{src}$, where each emits n_k particles. The average number of particles per source is then

$$n = \frac{1}{N_{src}} \sum_{k=1}^{N_{src}} \sum_{i=1}^{n_k} \frac{1}{N_{src}! \ 1} \int \hat{}_1(p) d^3p = ; \qquad (42)$$

where the overbar indicates an average over sources, and $\hat{}_1(p)$ is the particle momentum distribution per source in the limit of a continuum of all possible sources. In that limit, each source multiplicity has mean $= n$ and variance $^2 = \overline{n^2} \ \overline{n}^2$. Similarly, the distribution of

particle pairs emitted from one source is

$$\overline{n(n-1)} = \frac{1}{N_{src}} \sum_{k=1}^{N_{src}} \sum_{i=1}^{n_k} \sum_{j=i}^{n_k} 1 \qquad (43)$$

$$\to \int\int \hat{\rho}_2(p_1,p_2)\,d^3p_1\,d^3p_2 = \bar{n}^2 + \bar{n}_{src}; \quad N \to 1$$

where $\hat{\rho}_2(p_1,p_2)$ is the particle pair momentum distribution for an individual source.

The event averaged singles and pair momentum distributions become

$$\rho_1 = \langle \hat{\rho}_1(p) K \rangle \qquad (44)$$

and

$$\rho_2 = \langle \hat{\rho}_2(p_1,p_2) K + \hat{\rho}_1(p_1)\hat{\rho}_1(p_2) K(K-1) \rangle; \qquad (45)$$

where the angled brackets indicate the average over events and each event has K independent sources. Equation (44) species that the event multiplicity is a superposition of K sources, yielding

$$\langle N \rangle = \langle K \rangle \bar{n}: \qquad (46)$$

Equation (45) indicates particle pairs are made up of the sum of pairs from the K individual sources, each with $\hat{\rho}_2$ pairs, plus the sum of pairs where one particle of the pair is from one source and the other particle comes from a dierent source. For one pair of sources the particle pair distribution is $\hat{\rho}_1\hat{\rho}_1$, and there are $K(K-1)$ pairs of sources. The event average number of particle pairs then becomes

$$\langle N(N-1) \rangle = \langle K \rangle (\bar{n}^2 + \bar{n}_{src}) + \langle K^2 \rangle \bar{n}^2: \qquad (47)$$

Beginning with R as dened in (3) with (11), then using (44) and (45), we nd

$$R = \frac{R_s}{\langle K \rangle} + \frac{\langle K^2 \rangle - \langle K \rangle^2}{\langle K \rangle^2} \qquad (48)$$

where $R_s = (\bar{n}^2 - \bar{n})/\bar{n}^2$ is the equivalent of (30) for sources when averaging is done over the ensemble of all possible independent sources. Event-by-event uctua-tions in the number of sources are characterized by the variance of K in the rightmost term. Since the sources are taken to be independent, this variance follows Poisson statistics, so $\langle K^2 \rangle - \langle K \rangle^2 = \langle K \rangle$, and therefore uctua-tions (48) are diminished by $\langle K \rangle^{-1}$.

Two-particle correlations of transverse momentum, C, are dened by Eq. (4). Using Eq. (11) with (44) and (45) we nd

$$C = \frac{C_s}{\langle K \rangle} + \frac{\langle K^2 \rangle - \langle K \rangle^2}{\langle K \rangle^2} \langle p_t \rangle^2; \qquad (49)$$

where $C_s = (\bar{n}^2_{p_T} - \langle p_t \rangle)/\bar{n}^2$ is the equivalent of Eq. (35) for sources. Here the average total transverse momentum per source is dened as $P_T = \int \hat{\rho}_1(p)\, p_t\, dp$ and, using (44), the average total transverse momentum for events is $\langle P_T \rangle = \langle K \rangle P_T$. Following (18) and substituting (46), the event averaged transverse momentum per particle is equivalently written as

$$\langle p_t \rangle = P_T / \bar{n}: \qquad (50)$$

Finally, the variance of total transverse momenta per source is $\bar{n}^2_{p_T} = \overline{P_T^2} - P_T^2$, where $\int\int \hat{\rho}_2(p_1,p_2)\, p_{t,1} p_{t,2}\, dp_1 dp_2 = \bar{n}^2_{P_T} + \bar{n}_{src} \langle p_t \rangle^2 - \bar{n} \langle p_t \rangle^2$.

Notice that both Eqs. (48) and (49) have similar contribution from the uctuation in the number of sources. Given that the sources are independent, (49) decreases with the inverse of the number of sources in the same way as (48). However, momentum correlations (49) are sensitive to the transverse expansion due to the correlation function weighting by p_t. We reiterate that when C is measured as dened in (4) and not dierentially in relative azimuthal angle or pseudorapidity, then eects form anisotropic ow are eliminated. C then represents the magnitude of transverse momentum correlations generated in the reball. A measured deviation from predictions of the independent source model might suggest that sources of correlations are not independent, as would be the case for a partially or fully equilibrated system.

Multiplicity-momentum correlations, D, are dened by (1). Following the same procedure we use for R and C, we obtain

$$D = \frac{D_s}{\langle K \rangle} \qquad (51)$$

where $D_s = \mathrm{Cov}(P_T, n) / \langle p_t \rangle \bar{n}^2$ is the equivalent of Eq. (21) for sources rather than events.

Notice that since (21) is constructed to remove the effects of multiplicity uctuations, (51) does not have the same dependence on source uctuations as R or C. However, all three observables R, C, and D still are reduced by the inverse of the number of sources.

Lastly, correlations of transverse momentum uctuations are dened by (2). Again, using Eq. (11) with (44) and (45) we nd

$$\langle p_{t1} p_{t2} \rangle = \frac{\langle K \rangle C_s - 2\langle p_t \rangle D_s - \langle p_t \rangle^2 R_s}{\langle K \rangle R_s + \langle K^2 \rangle - \langle K \rangle} \qquad (52)$$

$$= \frac{\langle p_{t1} p_{t2} \rangle_s}{\langle K \rangle} \frac{(1+R_s)}{(1+R)}: \qquad (53)$$

Here $(1+R_s)\langle p_{t1} p_{t2} \rangle_s = C_s - 2\langle p_t \rangle D_s - \langle p_t \rangle^2 R_s$ following the same reasoning leading to Eq. (5) except that averaging is done over the ensemble of all possible independent sources rather than events. The denominator of (2) is dierent from the other observables in this work, but since $\langle p_{t1} p_{t2} \rangle$ is well studied in literature, this form better suits direct comparison to measured data. The consequence is that the eects from uctuating independent sources are not as obvious as the other observables. By examining (52) we see that $\langle p_{t1} p_{t2} \rangle$ approximately decreases like $\langle K \rangle^{-1}$ in the limit of large K where R is small.

If we take the origin of the sources to be participant nucleons, then the minimum number of sources in any collision is two. Calculations of R_s, C_s, D_s, and $\langle p_{t1} p_{t2} \rangle_s$ in proton-proton collisions can serve as a possible representation of independent source correlations. In this scenario, pp collisions always have $K = 2$ and never have a variance in the number of sources. Therefore we must have $\langle K^2 \rangle - \langle K \rangle^2 = 0$ in (48) and (49). Taking (48) as an example for pp collisions, we have $R_{pp} = R/2$ for $K = 2$ participants. Consequentially for AA collisions using $K = N_{part}$ and $R_s = 2R_{pp}$, we find Eq. (54). Similarly, Eqs. (48), (49), (51), and (53) become

$$R = \frac{2R_{pp}}{\langle N_{part} \rangle} + \frac{\langle N_{part}^2 \rangle - \langle N_{part} \rangle^2}{\langle N_{part} \rangle^2} \tag{54}$$

$$C = \frac{2C_{pp}}{\langle N_{part} \rangle} + \left(\frac{\langle N_{part}^2 \rangle - \langle N_{part} \rangle^2}{\langle N_{part} \rangle^2} \right) \langle p_t \rangle^2 \tag{55}$$

$$D = \frac{2D_{pp}}{\langle N_{part} \rangle} \tag{56}$$

$$\langle p_{t1} p_{t2} \rangle = \frac{2\langle p_{t1} \rangle_{pp} \langle p_{t2} \rangle_{pp}}{\langle N_{part} \rangle} \left(\frac{1 + R_{pp}}{1 + R} \right) \tag{57}$$

where R in the denominator of (57) must come from (54).

In this work we attribute all volume fluctuations to source fluctuations. To see how multiplicity fluctuations are influenced by volume (source) fluctuations, imagine that the variance of the number of participants in the numerator of the rightmost term of (54) follows Poisson statistics. Then $Var(N_{part}) = \langle N_{part} \rangle$ and (54) becomes $R = (2R_{pp} + 1)/\langle N_{part} \rangle$. Note that the contribution from genuine source correlations is represented by $2R_{pp}$. If $2R_{pp} = 1$, then half of multiplicity fluctuations come from genuine correlations and half come from source fluctuations. If $2R_{pp} < 1$, then source fluctuations contribute more to R than genuine correlations. If $2R_{pp} > 1$, then source fluctuations contribute less to R than genuine correlations We estimate R_{pp} using PYTHIA simulations and list values in Table I for $\sqrt{s} = 200$ GeV and $\sqrt{s} = 2.76$ TeV collision energies. At $\sqrt{s} = 200$ GeV, a bit less than two thirds of R comes from source fluctuations. At $\sqrt{s} = 2.76$ TeV, about half of R comes from source fluctuations.

Transverse momentum correlations, (55), have similar dependence on source fluctuations. For a Poissonian distribution of participant sources we have $C = (2C_{pp} + \langle p_t \rangle^2)/\langle N_{part} \rangle$. Genuine correlations and source fluctuations have equal contributions to C when $2C_{pp} = \langle p_t \rangle^2$. Using values from Table I we find that at the contributions to C from genuine correlations and source fluctuations are roughly equal but source fluctuations are slightly larger at $\sqrt{s} = 200$ GeV and genuine correlations are slightly larger at $\sqrt{s} = 2.76$ TeV. We leave an analysis of collision energy dependence to future work.

IX. RESULTS FROM SIMULATION

In this section, our primary goal is to make the first estimates of D and test relationship (5) with simulated collision events. We do not attempt to preform a comprehensive study using different simulation routines to compare different collision dynamics mechanisms; we leave this for future work. For simplicity, we chose PYTHIA 8.2 [46] since its description of pp collisions is well established and it includes the Angantyr model for nuclear collisions [47] which provides a baseline estimation based on wounded nucleons.

We look for non-zero values of the new observable D, defined by equations (1) or (24). D indicates a multiplicity-momentum correlation and possibly a deviation from thermal equilibrium, see Sec. IV. Moreover, we also test the $1/\langle N \rangle$ dependence of (1), (2), (3), and (4) when using multiplicity as a centrality measure. Deviation from this trend is an indication of non-Poissonian particle production, meaning correlations develop between particles emerging from different sources, or other correlation mechanisms.

When measuring correlations based on moments of a multiplicity distribution, centrality biases can be significant, especially when the same particles used to calculate the correlations are also used to determine centrality [78]. To eliminate centrality biases due to volume fluctuations, we follow the centrality method of Ref. [30] when calculating observable dependencies on multiplicity. This method allows for one-particle-wide multiplicity bins without encountering the biases described at the end of Sec. V.

In this method, observables are calculated using all charged particles in the mid-rapidity region $|\eta| < 0.5$ while centrality is determined using all charged particles in the remaining region of experimental rapidity acceptance. We label these accepted centrality determining particles N_{acc}. For comparison to STAR, charged particles in the region $0.5 < |\eta| < 1.0$ are used for N_{acc}. For comparison to ALICE, charged particles in the region $0.5 < |\eta| < 0.8$ are used for N_{acc}. In Figs. 6 and 7 we plot the average mid-rapidity multiplicity vs N_{acc} in PYTHIA events. The acceptance difference between STAR and ALICE accounts for the different slopes in the mid-rapidity multiplicities. This centrality measure also has the consequence of transforming the two-particle correlation observables into three-particle correlations since two particles are used to calculate the correlation and different particles are used to determine N_{acc}. If the pseudorapidity distribution of charged particles is approximately at in the rapidity acceptance, then the correlation between the number of particles in the centrality determining and mid-rapidity regions is effectively 1, and multiplicity trends can be taken at face value.

A nonlinear correlation between N_{acc} and the mid-rapidity multiplicity could induce some modulation in correlation measurements away from the expected $1/\langle N \rangle$ trend. However, the average mid-rapidity multiplicity

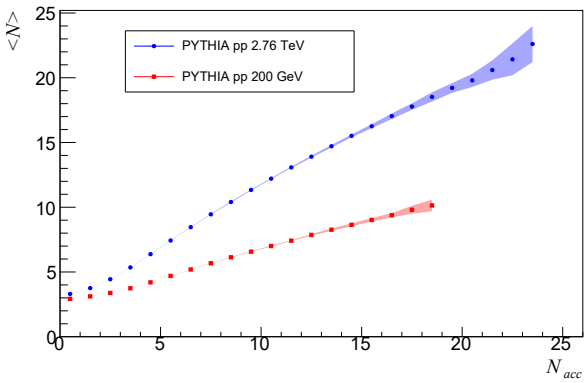

FIG. 6. Sub-group averaged mid-rapidity multiplicity hNi as a function of accepted multiplicity N_{acc} in the region 0:5 < jj < 1:0 for pp 200 GeV and 0:5 < jj < 0:8 for pp 2.76 TeV.

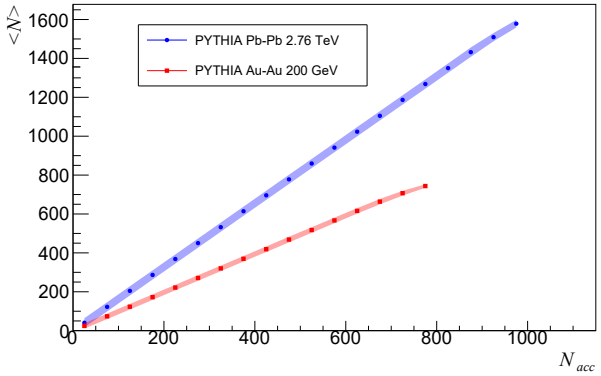

FIG. 7. Sub-group averaged mid-rapidity multiplicity hNi as a function of accepted multiplcity N_{acc} in the region 0:5 < jj < 1:0 for Au-Au 200 GeV and 0:5 < jj < 0:8 for Pb-Pb 2.76 TeV.

hNi tracks very linearly with N_{acc} for PYTHIA events in Figs. 6 and 7 for pp and AA collisions respectively.

Similarly to Ref. [30], we employ the so-called "sub-group" method for estimating the uncertainty of correlation observables. In our analysis, the full set of events for a given centrality class is divided up into 30 sub-groups and all observables are calculated for each sub-group. Each observable is then averaged over all sub-groups and the standard deviation is used to estimate the uncertainty. For AA collisions, when multiplicity is used for centrality and after taking the sub-group average, we average observable values over several multiplicity bins and the set the error band to represent the standard deviation of those values.

In Figs. 4 and 5 we report the average transverse momentum per particle from PYTHIA events in select pp and AA systems and energies. For all PYTHIA simulation results we show in this work, we have used both the centrality and sub-group methods described above. Notice the increase in p_t per particle as multiplicity increases in both gures. We will later argue that this is important for understanding multiplicity-momentum correlations D. The smaller increase in AA collisions compared to pp collisions is likely a factor in the dier-ent magnitudes of D estimates from dierent collision systems.

We now turn to estimating observables R, C, $hp_{t1}p_{t2}i$, and D, and their mathematical relationship (5) with PYTHIA simulations of pp and AA collision systems at select energies. For the four observables we analyze events following (30), (35), (12), and (21) respectively. We use the kinematic ranges 0:15 < p_t < 2 GeV and jj < 1 for Au-Au collisions at $\sqrt{s}$ = 200 GeV and jj < 0:8 for Pb-Pb collisions at $\sqrt{s}$ = 2:76 TeV. To identify deviation from 1=hNi behavior we plot the product of each observable with the multiplicity hNi. If there is no deviation from $1=h^{N}i$, then results will be constant with multiplicity, though with dierent magnitudes.

Multiplicity uctuations, attributed to volume uctuations, R, are dened by (3) or (30). Results for hNiR from PYTHIA simulation of pp collisions at 200 GeV and 2:76 TeV are shown in Fig. 8(a). At lower multiplicities, deviation from 1=hNi behavior is likely the result of a small variance of total multiplicity produced in these events. Similarly in the very low multiplicity region, values become negative. Consider that events with very few particles in the centrality dening rapidity region also have correspondingly very few particles in the mid-rapidity region. In this case the variance of mid-rapidity particles is nearly zero. Following the argument surrounding Eq. (34), negative values of R can be expected. At larger multiplicities hNiR becomes more at and the error band increases with the scarcity of events. It is interesting to note that hNiR in pp collisions at $\sqrt{s}$ = 2:76 TeV indicates a slightly faster than 1=hNi decrease with increasing multiplicity when compared to $\sqrt{s}$ = 200 GeV collisions. It will be interesting to discover if this change persists to higher or lower collision energies in both simulation and experiment. Moreover, it is also signicant to point out that hNiR is non-zero, which indicates that particle production { averaged over events { is not Poissonian and therefore not independent. This reinforces the fact that R measures a fundamental particle production mechanism. Deviation of experimental measurements from PYTHIA estimates could signal the contribution form dierent particle sources. A comparison covering dierent collision systems and energies may be a useful tool to characterize the onset of QGP or jet inuences on particle production.

Results for hNiR from PYTHIA/Angantyr simulation of Au-Au and Pb-Pb collisions at $\sqrt{s}$ = 200 GeV and $\sqrt{s}$ = 2:76 TeV are shown in Fig. 9(a), plotted versus multiplicity. When centrality is determined by multiplicity, hNiR is seemingly constant until the most central points. The deviation in high multiplicity events is likely due to low statistics. The drop of the lowest multiplicity point is the result of averaging the rst few lowest multiplicity bins where values may be small or negative for the same reasons small or negative values appeared in low

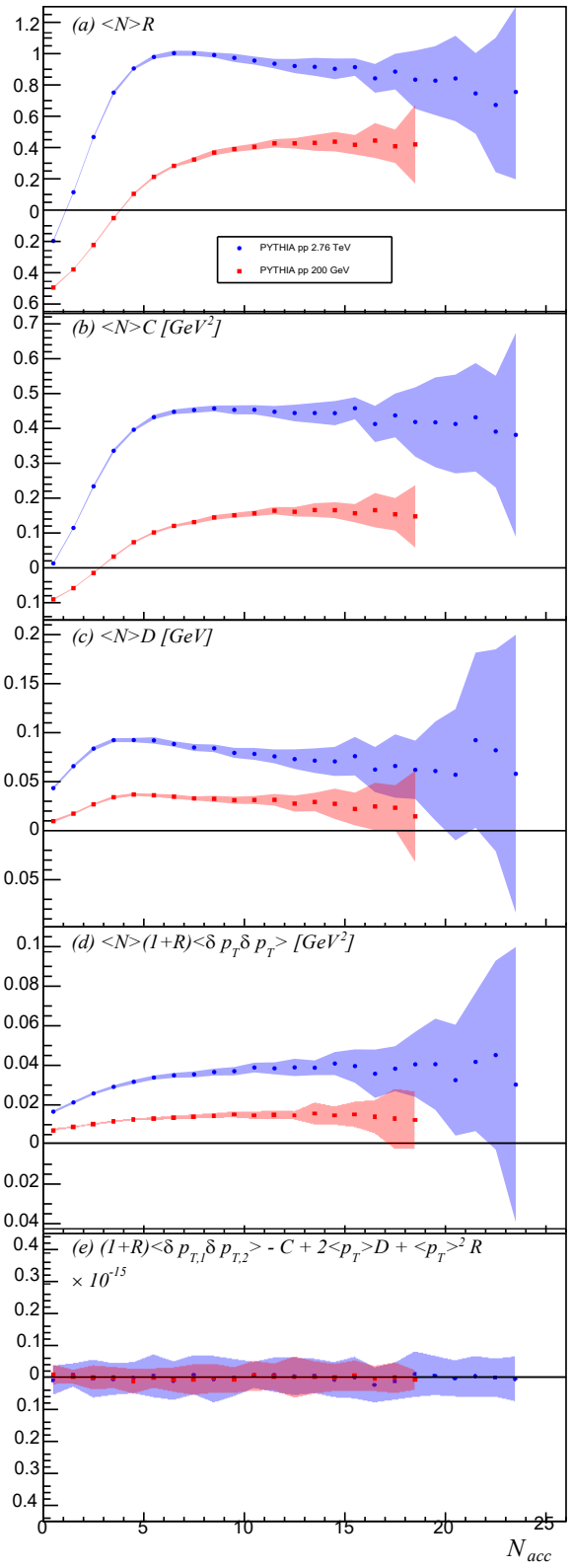

FIG. 8. Calculation of observables (1), (2), (3), and (4), scaled by mid-rapidity multiplicity hNi using PYTHIA pp collisions.

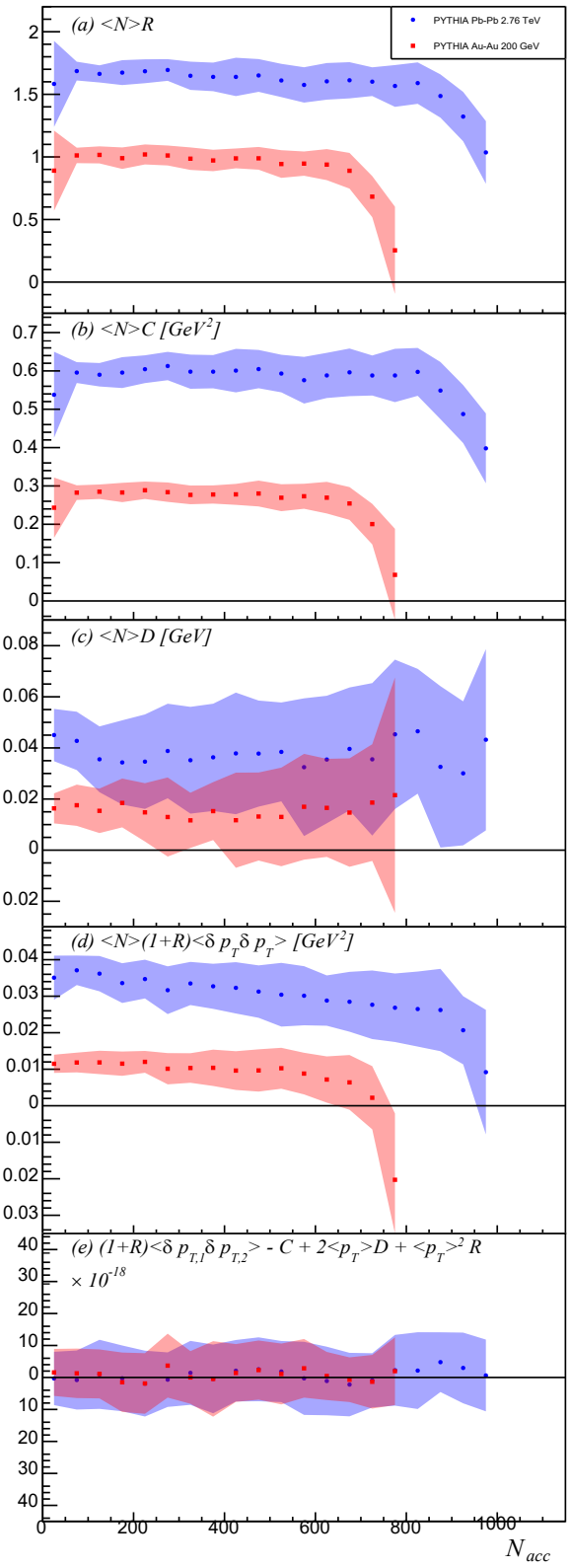

FIG. 9. Calculation of observables (1), (2), (3), and (4), scaled by mid-rapidity multiplicity hNi using PYTHIA/Angantyr AA collisions.

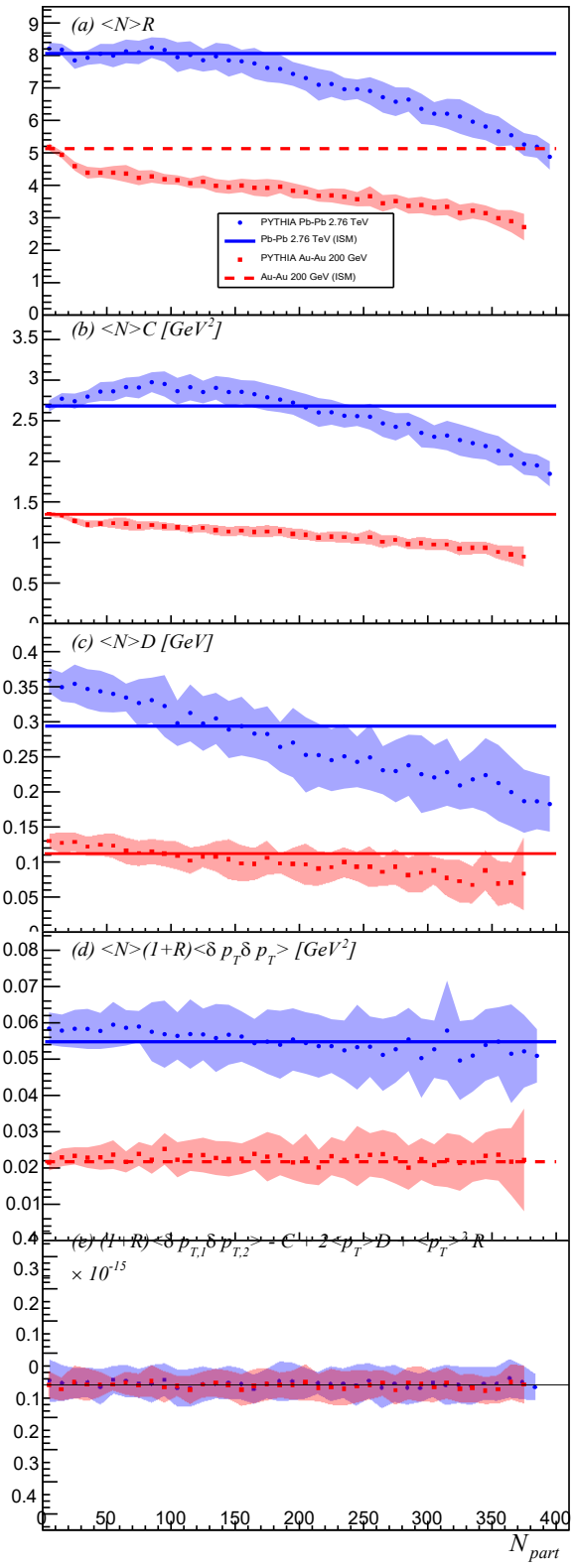

FIG. 10. Calculation of observables (1), (2), (3), and (4), scaled by multiplicity hNi using PYTHIA/Angantyr AA collisions. Solid lines represent the wounded nucleon model.

TABLE I. List of integrated values of observables $\langle N \rangle_{pp}$, $\langle p_t \rangle_{pp}$, (30), (35), (12), and (21) using PYTHIA pp collision events calculated with the sub-group method. Calculations are made with charged particles from the kinematic region and $|\eta| < 0.8$ ($\sqrt{s} = 2.76$ TeV) or $|\eta| < 1.0$ ($\sqrt{s} = 200$ GeV). Listed uncertainties are the standard deviation of the sub-group values.

$\sqrt{s}$	200 GeV		2.76 TeV	
	6.635	3.6510 ^{3}		8.1010 ^{3}
$\langle N \rangle_{pp}$	0.4860	1.3310 ^{4}	8.453	1.7810 ^{4}
$\langle p_t \rangle_{pp}$	0.2731	7.5810 ^{4}	0.5356	1.0210 ^{3}
R_{pp}	0.0842	2.2010 ^{4}	0.453	4.8410 ^{4}
C_{pp}	0.00257	2.2710 ^{5}	0.1738	3.6710 ^{5}
$\langle p_{t1} p_{t2} \rangle_{pp}$	0.01685	9.3210 ^{5}	0.00446	1.6810 ^{4}
D_{pp}			0.0348	

multiplicity pp collisions. In general, the approximately constant value of $\langle N \rangle R$ with multiplicity is consistent with a superposition of pp sub-collision model.

To test the Independent Source Model, the same quantity, $\langle N \rangle R$, is plotted with respect to the number of participating nucleons (N_{part}) and is shown in Fig. 10(a). Taking participating nucleons as the sources of particles, we plot (54) as the solid and dashed lines on the gure. We assume that the variance of N_{part} in (54) is Poissonian and reduces the rightmost term to $1/\langle N_{part} \rangle$. Also using PYTHIA, we calculate the \integrated" value R_{pp} including all pp events without centrality constraints. Values for pp collisions at $\sqrt{s} = 200$ GeV and $\sqrt{s} = 2.76$ TeV are listed in Table I. When dening centrality with N_{part}, we use the full experimental rapidity acceptance to calculate all observables and the same is done for integrated values. Notice that when $N_{part} = 2$ on Fig. 10(a), Eq. (54) matches closely with the data, but deviates at larger N_{part}. This may indicate that the source value $R_s = 2R_{pp}$ is dominated by lower multiplicity pp events, or simply that participating nucleons, on their own, are not a good indicator of all particle sources. Momentum correlations, C, are dened by equations (4) or (35). Due to its similar construction, it shares many of the same centrality trends as R. C scales both with R and $\langle p_t \rangle^2$; the latter scaling is visible by examining (49). $\langle N \rangle C$ is reported on Figs. 8(b), 9(b), and 10(b). Centrality behaviors mostly follow those of $\langle N \rangle R$, except in Fig. 10(b). In comparison to our ISM for wounded nucleons in Pb-Pb collisions at $\sqrt{s} = 2.76$ TeV, $\langle N \rangle C$ increases from peripheral collisions peaking around N_{part} 100. This increase is not seen in $\langle N \rangle R$ for the same collision system. Additionally this peak is not seen for $\langle N \rangle C$ in Au-Au collisions at $\sqrt{s} = 200$ GeV.

The centrality dependence of C can be analyzed in the context of (40). Notice in Fig. 10(b) that $\langle N \rangle D$ and $\langle N \rangle (1 + R) \langle p_{t1} p_{t2} \rangle$ both exceed the wounded nucleon model expectation in the same region where $\langle N \rangle C$ peaks. Care should be taken when assigning meaning to the peak in Fig. 10(b): when $\langle N \rangle C$ is plotted with respect to multiplicity in Fig. 9(b), the peak behavior is not seen. There-

fore, we use these observations only as a tool to demonstrate the usefulness of measuring correlation observables as a complementary set with a mathematical connection like (5).

Correlations of transverse momentum uctuations, $\langle p_{t1} p_{t2} \rangle$, are dened by equations (2) or (12). STAR and ALICE have measured the similar form (14), usually reporting it as (20). In Fig. 1 we compare (20), calculated from both (12) and (14), with experimental data for pp collisions. The two methods (12) and (14) are in generally good agreement. Similar results are obtained for AA collisions but are omitted from Fig. 2 for clarity.

PYTHIA comparisons to experimental AA data are shown in Fig. 2. Agreement with STAR data is good but signicant dierence from ALICE data is seen. This is likely due to dierences in the multiplicity centrality determination between STAR and ALICE; our calculation technique reproduces that of [5]TAR.

To test the $1/\langle N \rangle$ dependence of $\langle p_{t1} p_{t2} \rangle$, we plot $\langle N \rangle (1 + R) \langle p_{t1} p_{t2} \rangle$ in Figs. 8(d), 9(d), and 10(d). As we discover in Secs. VII and VIII, the factor $(1 + R)$ is required to re-scale the normalization of (12) so that it follows the same $1/\langle N \rangle$ trend as the other observables.

PYTHIA results for $\langle N \rangle (1 + R) \langle p_{t1} p_{t2} \rangle$ in pp collisions, shown in Fig. 8(d), are mostly at except in peripheral collisions where uctuations become small. In AA collisions, shown in Fig. 9(d), the trend is again consistent, inside the error band, with a $1/\langle N \rangle$ except in the most central collisions that are statistically limited. $\langle p_{t1} p_{t2} \rangle$ has reduced eect from small uctuations at low multiplicity in comparison to R or C. By construc-tion, $\langle p_{t1} p_{t2} \rangle$ removes multiplicity uctuations (see the discussion following Eq. (38) in Sec. VII). Therefore, $\langle p_{t1} p_{t2} \rangle$ appears insensitive to choice of centrality via multiplicity or participating nucleons. Results in Fig. 10(d) for $\langle N \rangle (1^{+}R) \langle p_{t1} p_{t2} \rangle$ with respect to participat-ing nucleons are also constant and in strong agreement with the wounded nucleon model, Eq. (57).

The deviation of the wounded nucleon model in Fig. 3 in comparison to Fig. 10(d) is likely due to multiple factors. First, the integrated value of $\langle p_t \rangle_{pp}$ is used with (57). In the independent source model, $\langle p_t \rangle$ is the same for individual sources as it is for the whole event. $\langle p_t \rangle_{pp}$ does not change value in our simple wounded nucleon model, but $\langle p_t \rangle$ does change in the centrality dependent measurement. Last, the factor of $(1 + R)$ in the denominator of (57) also induces a dierence from PYTHIA values. As we see in Fig. 10(a), R for our wounded nucleon model is larger than PYTHIA values, particularly in more central collisions.

Multiplicity-momentum correlations, D, are dened by equations (1) or (21). An objective of this work is to stimulate experimental measurement of D. The rst estimates of $\langle N \rangle D$ from PYTHIA pp and AA collisions are shown in Figs. 8(c), 9(c), and 10(c). Immediate observations include that D = 0 and is positive. The positive nonzero value of D is consistent with $\langle p_t \rangle$ calculations. For example, notice in Fig. 4 that the average transverse momentum per particle increases with the number of particles. This is a multiplicity-momentum correlation. The dierence of magnitudes of $\langle N \rangle D$ in pp and AA collisions may be due to the fact that the rate of increase of $\langle p_t \rangle$ with multiplicity is greater in pp collisions that in AA for PYTHIA simulations.

The atness of $\langle N \rangle D$ with respect to centrality indicates agreement with the $1/\langle N \rangle$ dependence. Interestingly, pp collisions show a small negative slope with increasing multiplicity, indicating a faster than $1/\langle N \rangle$ drop with increasing multiplicity. This slope seems to increase from $\sqrt{s} = 200$ GeV to $\sqrt{s} = 2.76$ TeV collision energies. We look for experimental measurements in a larger range of collision energies to examine this behavior.

Figure 10(c) shows that when centrality is determined by participating nucleons, peripheral collisions have higher D values than determined by our wounded nucleon model. This may simply signal a dierence between our choice to use only participant nucleons as sources in our independent source model and the PYTHIA/Angantyr model. However, if that is true, then D is the most sensitive of the observables to this dierence.

D may also be sensitive to the thermalization of the medium. Similarly, we show in Ref. [34] that $\langle p_{t1} p_{t2} \rangle$ can be used to measure incomplete thermalization, then D as well as C may provide additional constraints on that model. We leave this to future work.

X. SUMMARY

In this work, we show that a set of four two-particle correlation observables R, C, $\langle p_{t1} p_{t2} \rangle$, and D are mathematically related by Eq. (5). When these observables are measured or calculated simultaneously with the same method, (5) can act as a validation tool or as a test for theoretical models. Importantly, since each observable signals a dierent aspect of the collision system, (5) can be used to estimate the relative eects of dierent physics on an individual observable.

In Sec. II, we briey discuss the construction of a general two-particle momentum density correlation function, Eq. (11). The four connected two-particle correlation observables (1), (2), (3), and (4) are all derived from this same common origin.

Multiplicity uctuations, R, dened by (30) in Sec. V, test particle production mechanisms. They are signicantly inuenced by centrality or volume uctuations implying a connection between the overlap of the collision region (this distribution of particle sources) and the number of produced particles. R is constructed such that if event multiplicity is completely independent event-to-event { where the produced particle distribution is Poissonian and the particle variance is equal to the mean { then R = 0. Non-zero R indicates that events in the same ensemble produce particles following a common underlying physics of particle production that induces an

event-by-event correlation. It is tempting to attribute this correlation to the geometrical initial state distribution of collision energy in nuclear collisions, but R is also non-zero in pp collisions. This might suggest that the initial state is more accurately described by sub-nucleon scale physics.

Multiplicity uctuations set the overall scale of the parent correlation function (11) for all observables discussed in this work. In the absence of correlation, R depends on multiplicity following $1=h^{N}i$. Positive values of R indicate a correlation such that the multiplicity variance is larger than hNi. Additionally, if the multiplicity variance does not increase proportionally with hNi, then R will deviate from a 1=hNi trend, which may signal QCD critical point uctuations or other novel physics. All two-particle correlations represented by (11) and normalized similarly to R should vary with centrality following these general properties. Therefore, we look for deviation from 1=hNi in all correlation observables.

Diculty in measuring R emerges when the same particles are used to calculate R and simultaneously dene centrality; this induces centrality bias eects that can be large. In our PYTHIA estimates in Sec. IX, we chose to follow centrality denitions used by STAR [30]. We calculate observables with charged particles in the region jj < 0:5 and determine centrality with charged particles in the region 0:5 < jj < $_{max}$ where $_{max}$ is the maxi-mum rapidity acceptance of either the STAR or ALICE detectors. Forward detector centrality determinations would provide an opportunity to measure correlations using particles in a larger central rapidity acceptance range. However, our goal in this work was to demonstrate the relationship (5) rather than explore all possible measurement techniques.

Dierential studies of R in relative rapidity and azimuthal angle led to the discovery of the ridge, which shows that correlations extend to large separations in rapidity. Various explanations attribute the appearance of the ridge to ow or other correlations modied by ow, but geometrical correlations alone would yield a value of R = 0 when integrated. We nd the integrated vale of R to be non-zero in PYTHIA pp and AA events. This fact shapes the interpretation of all two-particle correla-tions in this work. In particular, a \non-ow" correlation is sensitive to the particle production mechanism as well as the thermalization process.

Momentum correlations, C, dened by (35) in Sec. VI, are the transverse momentum weighted equivalent of R. Because of the momentum weighting, these correlations are sensitive to dynamical forces during the evolution of the collision system, like viscosity, in addition to the initial state eects that generate R.

Correlations of transverse momentum uctuations, $hp_{t1}p_{t2}i$, dened by (12) in Sec. III have been widely studied as a measure of collision system dynamics, temperature uctuations, and critical point phase change phenomenon. New in this work, through (5), or equivalently (38), we show how momentum correlations, multiplicity uctuations, and momentum-multiplicity correlations all separately contribute to $hp_{t1}p_{t2}i$. Equation (38) also highlights how $hp_{t1}p_{t2}i$ is stable against changes in centrality denition in comparison to other correlation observables. Since C contains the same number density uctuations as R, the dierence C $hp_t iR$ in (38) essentially removes the number density uctuations corresponding to their common centrality denition.

Also new in this work is the denition of a measure of multiplicity-momentum correlations, D, dened by (21). In Sec. IV, we estimate that, in the Grand Canonical Ensemble, D = 0. Conversely in Sec. IX, we calculate a positive value from PYTHIA simulations that is comparable in magnitude to $hp_{t1}p_{t2}i$. PYTHIA simulations do not contain bulk correlation dynamics, and we argue that a positive multiplicity-momentum correlation is supported by the increasing value of the average transverse momentum per particle with increasing multiplicity in both pp and AA collision systems. Taken together, these observations suggest that D is sensitive to both particle production and equilibration mechanisms. We plan to address the issue of equilibration in future work that extends on our results in Ref. [34].

In Sec. IX we calculate estimates of the observables with PTYHIA/Angantyr which contains no bulk collectivity or QGP phase. Our purpose is to demonstrate the usefulness of (5) and make rst estimates of D. We leave a more expansive study of dierent event simulation routines and their dierent physics for future work. To examine 1=hNi scaling, we plot hNiR, hNiC, hNiD, and $hNi(1 + R)hp_{t1}p_{t2}i$. As discussed in Sec. VII, we note that the factor of (1 + R) is needed to re-scale the normalization of $hp_{t1}p_{t2}i$ to have the expected 1=hNi dependence on multiplicity. We nd that, within errors, all observables basically follow a 1=hNi trend with multiplicity in PYTHIA events. Deviations are seen in low multiplicity pp systems where uctuations are small. We also nd that the relationship (5) is satised to a preci-sion of 10^{16} or better.

In Sec. VIII we calculate the observables (1), (2), (3), and (4) in an independent source model. Equations (48), (49), (51), and (52) support the 1=hNi dependence of the observables if total multiplicity results form the sum of individual source multiplicities. Equations (48) and (49) also show that R and C are can be dominated by source uctuations. This suggests that these observables can be used to distinguish systems with dierent initial states that have fundamentally dierent particle production mechanisms.

Particle sources can come from many dierent phys-ical mechanisms, but for simplicity we choose to test only the wounded nucleon model. Dierence between PYTHIA/Angantyr results for AA collisions and our wounded nucleon calculation are likely due to the dierences in the Angantyr nucleon-nucleon sub-collision superposition model and our choice of simple participant nucleon sources. Interestingly, D seems to be the most sensitive of the observables to this dierence.

We also demonstrate that (5) can be used to distinguish dierences in centrality trends between C and R. Though R is always constant or decreasing with N_{part}, C has a small non-monotonic rise at lower participants. We note that this rise is due to $hp_{t1}p_{t2}i$ and D contributions to momentum correlations and advocate for similar measurements in real experimental systems.

In conclusion, we show that two-particle multiplicity uctuations, transverse momentum correlations, correlations of transverse momentum uctuations, and multiplicity-momentum correlations are all derived from the same parent correlation function and mathematically connected by (5). We have estimated these observables and their connection with PYTHIA/Angantyr simulated collisions events at $\sqrt{s}$ = 200 GeV and $\sqrt{s}$ = 2:76 TeV collision energies. Multiplicity-momentum correlations are a new observable estimated here for the rst time. We propose that this collection of observables and their mathematical relationship, measured or calculated simultaneously, can provide more information than the sum of the individual measurements. Measurements of these observables over a wide range of collision systems and energies may provide invaluable information about initial state particle production mechanisms of hadronic collisions as well as the subsequent equilibration process in the collision medium.

ACKNOWLEDGMENTS

This work is supported in part by NSF-PHY1913005 (G.M. and M.K.). G.M. would like to give special thanks to undergraduates Alec Ferensic, Reinali Calisin, and Neil Fraylick for assistance in this work.

[1] S. Jeon and V. Koch, Charged particle ratio uctuation as a signal for QGP, Phys. Rev. Lett. 85, 2076 (2000), arXiv:hep-ph/0003168.
[2] M. Asakawa, U. W. Heinz, and B. Muller, Fluctuation probes of quark deconnement, Phys. Rev. Lett. 85, 2072 (2000), arXiv:hep-ph/0003169.
[3] V. Koch, M. Bleicher, and S. Jeon, Event-by-event uctuations and the QGP, Nucl. Phys. A 698, 261 (2002), arXiv:nucl-th/0103084.
[4] J. Adams et al. (STAR), Multiplicity uctuations in Au+Au collisions at s(NN)**(1/2) = 130-GeV, Phys. Rev. C 68, 044905 (2003), arXiv:nucl-ex/0307007.
[5] M. Zhou and J. Jia, Centrality uctuations in heavy-ion collisions, Phys. Rev. C 98, 044903 (2018), arXiv:1803.01812 [nucl-th].
[6] H. Heiselberg and A. D. Jackson, Anomalous multiplicity uctuations from phase transitions in heavy ion collisions, Phys. Rev. C 63, 064904 (2001), arXiv:nucl-th/0006021.
[7] K. Adcox et al. (PHENIX), Net charge uctuations in Au+Au interactions at s**(1/2) = 130-GeV, Phys. Rev. Lett. 89, 082301 (2002), arXiv:nucl-ex/0203014.
[8] J. Zaranek, Measures of charge uctuations in nuclear collisions, Phys. Rev. C 66, 024905 (2002), arXiv:hep-ph/0111228.
[9] S. Mrowczynski, Hadronic matter compressibility from event by event analysis of heavy ion collisions, Phys. Lett. B 430, 9 (1998), arXiv:nucl-th/9712030.
[10] A. Adare et al. (PHENIX), Charged hadron multiplicity uctuations in Au+Au and Cu+Cu collisions from $\sqrt{s_{NN}}$ = 22:5 to 200 GeV, Phys. Rev. C 78, 044902 (2008), arXiv:0805.1521 [nucl-ex].
[11] M. Mukherjee (ALICE), Event-by-event multiplicity uctuations in Pb-Pb collisions in ALICE, Acta Phys. Polon. Supp. 9, 283 (2016), arXiv:1603.06824 [hep-ex].
[12] F. Becattini, A. Keranen, L. Ferroni, and T. Gabbriellini, Multiplicity uctuations in the hadron gas with exact conservation laws, Phys. Rev. C 72, 064904 (2005), arXiv:nucl-th/0507039.
[13] S. Gavin and C. Pruneau, Covariance of anti-proton yield and source size in nuclear collisions, Phys. Rev. C 61, 044901 (2000).
[14] S. Gavin and J. I. Kapusta, Kaon and pion uctuations from small disoriented chiral condensates, Phys. Rev. C 65, 054910 (2002), arXiv:nucl-th/0112083.
[15] S. Mrowczynski, Measuring charge uctuations in high-energy nuclear collisions, Phys. Rev. C 66, 024904 (2002), arXiv:nucl-th/0112007.
[16] C. Pruneau, S. Gavin, and S. Voloshin, Methods for the study of particle production uctuations, Phys. Rev. C 66, 044904 (2002), arXiv:nucl-ex/0204011.
[17] H. Appelshauser et al. (NA49), Event-by-event uctuations of average transverse momentum in central Pb + Pb collisions at 158-GeV per nucleon, Phys. Lett. B 459, 679 (1999), arXiv:hep-ex/9904014.
[18] T. Anticic et al. (NA49), Transverse momentum uctuations in nuclear collisions at 158-A-GeV, Phys. Rev. C 70, 034902 (2004), arXiv:hep-ex/0311009.
[19] J. Adams et al. (STAR), Event by event < p(t) > uctuations in Au - Au collisions at s(NN)**(1/2) = 130-GeV, Phys. Rev. C 71, 064906 (2005), arXiv:nucl-ex/0308033.
[20] J. Adams et al. (STAR), Incident energy dependence of pt correlations at RHIC, Phys. Rev. C 72, 044902 (2005), arXiv:nucl-ex/0504031.
[21] D. Adamova et al. (CERES), Event by event uctuations of the mean transverse momentum in 40, 80 and 158 A GeV / c Pb - Au collisions, Nucl. Phys. A 727, 97 (2003), arXiv:nucl-ex/0305002.
[22] J. Adams et al. (STAR), Transverse-momentum p(t) correlations on (eta, phi) from mean-p(t) uctuations in Au-Au collisions at s(NN)**1/2 = 200-GeV, J. Phys. G 32, L37 (2006), arXiv:nucl-ex/0509030.
[23] J. Adams et al. (STAR), The Energy dependence of p_t angular correlations inferred from mean-p(t) uctuation scale dependence in heavy ion collisions at the SPS and RHIC, J. Phys. G 34, 451 (2007), arXiv:nucl-ex/0605021.
[24] K. Adcox et al. (PHENIX), Event-by-event uctuations in mean p(T) and mean e(T) in s(NN)**(1/2) = 130-GeV Au+Au collisions, Phys. Rev. C 66, 024901 (2002), arXiv:nucl-ex/0203015.
[25] S. Adler et al. (PHENIX), Measurement of nonrandom event by event uctuations of average transverse momen-

tum in s(NN)**(1/2) = 200-GeV Au+Au and p+p collisions, Phys. Rev. Lett. 93, 092301 (2004), arXiv:nucl-ex/0310005.
[26] B. B. Abelev et al. (ALICE), Event-by-event mean p_T uctuations in pp and Pb-Pb collisions at the LHC, Eur. Phys. J. C 74, 3077 (2014), arXiv:1407.5530 [nucl-ex].
[27] S. Heckel (ALICE), Event-by-event mean pT uctuations in pp and Pb{Pb collisions at the LHC, EPJ Web Conf. 90, 08006 (2015), arXiv:1502.00537 [nucl-ex].
[28] J. Adam et al. (ALICE), Flow dominance and factorization of transverse momentum correlations in Pb-Pb collisions at the LHC, Phys. Rev. Lett. 118, 162302 (2017), arXiv:1702.02665 [nucl-ex].
[29] S. Acharya et al. (ALICE), Two particle dierential transverse momentum and number density correlations in p-Pb and Pb-Pb at the LHC, Phys. Rev. C 100, 044903 (2019), arXiv:1805.04422 [nucl-ex].
[30] J. Adam et al. (STAR), Collision-energy dependence of p_t correlations in Au + Au collisions at energies available at the BNL Relativistic Heavy Ion Collider, Phys. Rev. C 99, 044918 (2019), arXiv:1901.00837 [nucl-ex].
[31] S. Gavin and G. Moschelli, Fluctuation Probes of Early-Time Correlations in Nuclear Collisions, Phys. Rev. C 85, 014905 (2012), arXiv:1107.3317 [nucl-th].
[32] S. Gavin, Partial thermalization in ultrarelativistic heavy ion collisions, Nucl. Phys. B351, 561 (1991).
[33] S. Gavin, Traces of thermalization from transverse momentum uctuations in nuclear collisions, Phys. Rev. Lett. 92, 162301 (2004), arXiv:nucl-th/0308067.
[34] S. Gavin, G. Moschelli, and C. Zin, Boltzmann-Langevin Approach to Pre-equilibrium Correlations in Nuclear Collisions, Phys. Rev. C 95, 064901 (2017), arXiv:1612.07856 [nucl-th].
[35] S. Gavin and M. Abdel-Aziz, Measuring Shear Viscosity Using Transverse Momentum Correlations in Relativistic Nuclear Collisions, Phys.Rev.Lett. 97, 162302 (2006).
[36] H. Agakishiev et al. (STAR), Evolution of the dierential transverse momentum correlation function with centrality in Au+Au collisions at $\sqrt{s_{NN}}$ = 200 GeV, Phys. Lett. B 704, 467 (2011), arXiv:1106.4334 [nucl-ex].
[37] S. Acharya et al. (ALICE), Longitudinal and azimuthal evolution of two-particle transverse momentum correlations in Pb-Pb collisions at $\sqrt{s_{NN}}$ = 2.76 TeV, Phys. Lett. B 804, 135375 (2020), arXiv:1910.14393 [nucl-ex].
[38] V. Gonzæez (ALICE), Characterizing the medium created in Pb{Pb collisions at by means of the evolution of two-particle transverse momentum correlations, J. Phys. Conf. Ser. 1602, 012010 (2020).
[39] V. Gonzalez, S. Basu, P. Ladron De Guevara, A. Marin, J. Pan, and C. A. Pruneau, Extraction of the spe-cic shear viscosity of quark-gluon plasma from two-particle transverse momentum correlations, (2020), arXiv:2012.10542 [nucl-ex].
[40] V. Gonzalez, A. Marin, P. Ladron De Guevara, J. Pan, S. Basu, and C. Pruneau, Eect of centrality bin width corrections on two-particle number and transverse momentum dierential correlation functions, Phys. Rev. C 99, 034907 (2019), arXiv:1809.04962 [physics.data-an].
[41] N. Magdy, S. Basu, V. Gonzalez, A. Marin, O. Evdokimov, R. A. Lacey, and C. Pruneau, Azimuthal dependence of two-particle transverse momentum current correlations, (2021), arXiv:2105.07912 [nucl-th].
[42] S. Gavin, G. Moschelli, and C. Zin, Rapidity Correlation Structure in Nuclear Collisions, Phys. Rev. C 94, 024921 (2016), arXiv:1606.02692 [nucl-th].
[43] G. Moschelli and S. Gavin, Measuring the Rate of Isotropization of Quark-Gluon Plasma Using Rapidity Correlations, Nucl. Phys. A 982, 311 (2019), arXiv:1807.06532 [nucl-th].
[44] G. Moschelli and S. Gavin, Extracting the Shear Relaxation Time of Quark{Gluon Plasma from Rapidity Correlations, Acta Phys. Polon. B 50, 1139 (2019).
[45] C. D. Zin, Dynamic uctuations from hydrodynamics and kinetic theory in high energy collisions, Ph.D. the-sis, Wayne State U., Detroit (2017).
[46] T. Sjøstrand, S. Ask, J. R. Christiansen, R. Corke, N. Desai, P. Ilten, S. Mrenna, S. Prestel, C. O. Rasmussen, and P. Z. Skands, An introduction to PYTHIA 8.2, Comput. Phys. Commun. 191, 159 (2015), arXiv:1410.3012 [hep-ph].
[47] C. Bierlich, G. Gustafson, L. Lønnblad, and H. Shah, The Angantyr model for Heavy-Ion Collisions in PYTHIA8, JHEP 10, 134, arXiv:1806.10820 [hep-ph].
[48] S. Voloshin and Y. Zhang, Flow study in relativistic nuclear collisions by Fourier expansion of Azimuthal particle distributions, Z. Phys. C 70, 665 (1996), arXiv:hep-ph/9407282.
[49] N. Borghini, P. M. Dinh, and J.-Y. Ollitrault, A New method for measuring azimuthal distributions in nucleus-nucleus collisions, Phys. Rev. C 63, 054906 (2001), arXiv:nucl-th/0007063.
[50] S. A. Voloshin, A. M. Poskanzer, and R. Snellings, Collective phenomena in non-central nuclear collisions, Landolt-Bornstein 23, 293 (2010), arXiv:0809.2949 [nucl-ex].
[51] P. M. Dinh, N. Borghini, and J.-Y. Ollitrault, Eects of HBT correlations on ow measurements, Phys. Lett. B 477, 51 (2000), arXiv:nucl-th/9912013.
[52] M. A. Lisa, S. Pratt, R. Soltz, and U. Wiedemann, Femtoscopy in relativistic heavy ion collisions, Ann. Rev. Nucl. Part. Sci. 55, 357 (2005), arXiv:nucl-ex/0505014.
[53] N. Borghini, P. M. Dinh, and J.-Y. Ollitrault, Are ow measurements at SPS reliable?, Phys. Rev. C 62, 034902 (2000), arXiv:nucl-th/0004026.
[54] P. Danielewicz et al., Collective Motion in Nucleus-nucleus Collisions at 800-MeV/nucleon, Phys. Rev. C 38, 120 (1988).
[55] N. Borghini, Multiparticle correlations and momentum conservation in nucleus-nucleus collisions, PoS LHC07, 013 (2007), arXiv:0707.0436 [nucl-th].
[56] S. Gavin and G. Moschelli, Flow Fluctuations from Early-Time Correlations in Nuclear Collisions, Phys. Rev. C 86, 034902 (2012), arXiv:1205.1218 [nucl-th].
[57] S. Gavin, L. McLerran, and G. Moschelli, Long Range Correlations and the Soft Ridge in Relativistic Nuclear Collisions, Phys. Rev. C79, 051902 (2009), arXiv:0806.4718 [nucl-th].
[58] B. Alver and G. Roland, Collision geometry uctuations and triangular ow in heavy-ion collisions, Phys. Rev. C 81, 054905 (2010), [Erratum: Phys.Rev.C 82, 039903 (2010)], arXiv:1003.0194 [nucl-th].
[59] M. Rybczynski, Z. Wlodarczyk, and G. Wilk, Possible signal for critical point in hadronization process, Acta Phys. Polon. B 35, 819 (2004), arXiv:hep-ph/0305329.
[60] M. J. Tannenbaum, The distribution function of the event-by-event average p(T) for statistically independent emission, Phys. Lett. B 498, 29 (2001).
[61] Z. Xu, J. Liu, D. Wei, J. Huo, C. Zhang, and L. Huo,

Event-by-event mean-p_t uctuations from the AMPT model with a dynamical quark coalescence mechanism, J. Phys. G 47, 125102 (2020).

[62] E. Ferreiro, F. del Moral, and C. Pajares, Transverse momentum uctuations and percolation of strings, Phys. Rev. C 69, 034901 (2004), arXiv:hep-ph/0303137.

[63] P. Bozek, W. Broniowski, and S. Chatterjee, Transverse Momentum Fluctuations and Correlations, Acta Phys. Polon. Supp. 10, 1091 (2017), arXiv:1707.04420 [nucl-th].

[64] B. Abelev et al. (STAR), Systematic Measurements of Identied Particle Spectra in pp; d^+ Au and Au+Au Collisions from STAR, Phys. Rev. C 79, 034909 (2009), arXiv:0808.2041 [nucl-ex].

[65] B. B. Abelev et al. (ALICE), Multiplicity dependence of the average transverse momentum in pp, p-Pb, and Pb-Pb collisions at the LHC, Phys. Lett. B 727, 371 (2013), arXiv:1307.1094 [nucl-ex].

[66] T. Sjostrand and M. van Zijl, A Multiple Interaction Model for the Event Structure in Hadron Collisions, Phys. Rev. D 36, 2019 (1987).

[67] T. Sjostrand, Colour reconnection and its eects on precise measurements at the LHC (2013) arXiv:1310.8073 [hep-ph].

[68] J. Adams et al. (STAR), Minijet deformation and charge-independent angular correlations on momentum subspace (eta, phi) in Au-Au collisions at s(NN)**(1/2) = 130-GeV, Phys. Rev. C 73, 064907 (2006), arXiv:nucl-ex/0411003.

[69] J. Putschke (STAR), Intra-jet correlations of high-p_t hadrons from STAR, J. Phys. G 34, S679 (2007), arXiv:nucl-ex/0701074.

[70] A. Adare et al. (PHENIX), Dihadron azimuthal correlations in Au+Au collisions at $\sqrt{s_{NN}}$ = 200 GeV, Phys. Rev. C 78, 014901 (2008), arXiv:0801.4545 [nucl-ex].

[71] B. Alver et al. (PHOBOS), High p(T) Triggered Delta eta, Delta-phi Correlations over a Broad Range in Delta eta, J. Phys. G 35, 104080 (2008), arXiv:0804.3038 [nucl-ex].

[72] M. Sharma and C. A. Pruneau, Methods for the Study of Transverse Momentum Dierential Correlations, Phys. Rev. C 79, 024905 (2009), arXiv:0810.0716 [nucl-ex].

[73] S. Ravan, P. Pujahari, S. Prasad, and C. A. Pruneau, Correcting Correlation Function Measurements, Phys. Rev. C 89, 024906 (2014), arXiv:1311.3915 [nucl-ex].

[74] K. Aamodt et al. (ALICE), Harmonic decomposition of two-particle angular correlations in Pb-Pb collisions at $\sqrt{s_{NN}}$ = 2.76 TeV, Phys. Lett. B 708, 249 (2012), arXiv:1109.2501 [nucl-ex].

[75] P. Kovtun, D. T. Son, and A. O. Starinets, Viscos-ity in strongly interacting quantum eld theories from black hole physics, Phys. Rev. Lett. 94, 111601 (2005), arXiv:hep-th/0405231.

[76] S. A. Voloshin, Transverse radial expansion in nuclear collisions and two particle correlations, Phys. Lett. B 632, 490 (2006), arXiv:nucl-th/0312065.

[77] A. Dumitru, F. Gelis, L. McLerran, and R. Venugopalan, Glasma ux tubes and the near side ridge phenomenon at RHIC, Nucl. Phys. A 810, 91 (2008), arXiv:0804.3858 [hep-ph].

[78] X. Luo, J. Xu, B. Mohanty, and N. Xu, Volume uctuation and auto-correlation eects in the moment analysis of net-proton multiplicity distributions in heavy-ion collisions, J. Phys. G 40, 105104 (2013), arXiv:1302.2332 [nucl-ex].